Article

Mitochondrial ubiquinol oxidation is necessary for tumour growth

https://doi.org/10.1038/s41586-020-2475-6

Received: 16 December 2018

Accepted: 20 April 2020

Published online: 8 July 2020

Check for updates

Inmaculada Martínez-Reyes[1], Luzivette Robles Cardona[1], Hyewon Kong[1], Karthik Vasan[1], Gregory S. McElroy[1], Marie Werner[1], Hermon Kihshen[1], Colleen R. Reczek[1], Samuel E. Weinberg[1], Peng Gao[2], Elizabeth M. Steinert[1], Raul Piseaux[1], G. R. Scott Budinger[1] & Navdeep S. Chandel[1,3]✉

The mitochondrial electron transport chain (ETC) is necessary for tumour growth[1–6] and its inhibition has demonstrated anti-tumour efficacy in combination with targeted therapies[7–9]. Furthermore, human brain and lung tumours display robust glucose oxidation by mitochondria[10,11]. However, it is unclear why a functional ETC is necessary for tumour growth in vivo. ETC function is coupled to the generation of ATP—that is, oxidative phosphorylation and the production of metabolites by the tricarboxylic acid (TCA) cycle. Mitochondrial complexes I and II donate electrons to ubiquinone, resulting in the generation of ubiquinol and the regeneration of the NAD+ and FAD cofactors, and complex III oxidizes ubiquinol back to ubiquinone, which also serves as an electron acceptor for dihydroorotate dehydrogenase (DHODH)—an enzyme necessary for de novo pyrimidine synthesis. Here we show impaired tumour growth in cancer cells that lack mitochondrial complex III. This phenotype was rescued by ectopic expression of *Ciona intestinalis* alternative oxidase (AOX)[12], which also oxidizes ubiquinol to ubiquinone. Loss of mitochondrial complex I, II or DHODH diminished the tumour growth of AOX-expressing cancer cells deficient in mitochondrial complex III, which highlights the necessity of ubiquinone as an electron acceptor for tumour growth. Cancer cells that lack mitochondrial complex III but can regenerate NAD+ by expression of the NADH oxidase from *Lactobacillus brevis* (*Lb*NOX)[13] targeted to the mitochondria or cytosol were still unable to grow tumours. This suggests that regeneration of NAD+ is not sufficient to drive tumour growth in vivo. Collectively, our findings indicate that tumour growth requires the ETC to oxidize ubiquinol, which is essential to drive the oxidative TCA cycle and DHODH activity.

To genetically decipher the mechanism that underlies the necessity of the ETC for tumour growth, we used 143B osteosarcoma cells that are deficient in mitochondrial complex III. These cells contain a four-base-pair deletion of the cytochrome *b* gene (143B-*CYTB*-Δ; *CYTB* is also known as *MT-CYB*), which encodes an essential component of complex III. The loss of complex III function results in dysfunctional ETC, oxidative phosphorylation (OXPHOS), and DHODH activities (Extended Data Fig. 1a, b). These cells maintain their mitochondrial membrane potential by reversing mitochondrial complex V (ATP synthase) activity[14]. 143B-*CYTB*-Δ cells have a negligible oxygen consumption rate (OCR) (Fig. 1a) and OXPHOS (that is, coupled OCR) (Extended Data Fig. 1c). 143B-*CYTB*-Δ cells are auxotrophic for pyruvate and uridine in vitro[2]. They require pyruvate to maintain levels of aspartate, a key metabolite for tumour growth in vivo, by maintaining the NAD+/NADH ratio[15–18], and uridine to maintain pyrimidine synthesis through the salvage pathway in the absence of DHODH activity due to loss of complex III function[19]. In the absence of cell-permeable methyl pyruvate or uridine, 143B-*CYTB*-Δ cells are unable to maintain aspartate synthesis or proliferate (Extended Data Fig. 1d–f). As expected, the whole-cell NAD+/NADH ratio (which is the average of the cytosolic and mitochondrial pools) was significantly lower in 143B-*CYTB*-Δ cells in the absence of methyl pyruvate and uridine (Extended Data Fig. 1g). Regardless of the availability of pyruvate and uridine, 143B-*CYTB*-Δ cells display significant differences in metabolite levels compared with wild-type 143B cells (Extended Data Fig. 1h, i). Our previous studies have demonstrated that 143B-*CYTB*-Δ cells in vitro can sustain anchorage-independent growth in the presence of pyruvate and uridine through glutamine-dependent reductive carboxylation[2,20]. However, 143B-*CYTB*-Δ cells were unable to grow tumours in vivo, which highlights different growth phenotypes between the in vitro and in vivo environments (Fig. 1b, Extended Data Fig. 1j). To further confirm the necessity of complex III for tumour growth in immunocompetent mice, we used CRISPR–Cas9 gene editing

[1]Department of Medicine, Northwestern University Feinberg School of Medicine, Chicago, IL, USA. [2]Robert H. Lurie Cancer Center Metabolomics Core, Northwestern University Feinberg School of Medicine, Chicago, IL, USA. [3]Department of Biochemistry and Molecular Genetics, Northwestern University Feinberg School of Medicine, Chicago, IL, USA.
✉e-mail: nav@northwestern.edu

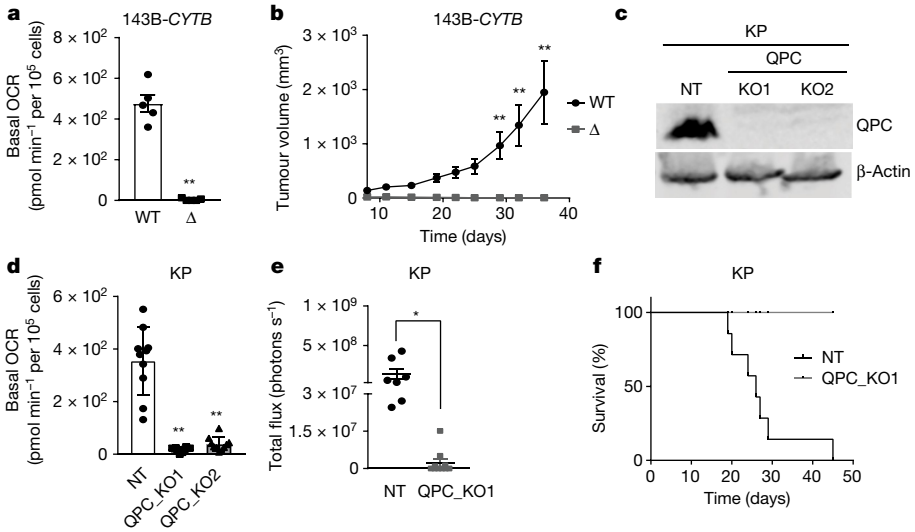

Fig. 1 | Complex III is necessary for tumour growth. a, Basal OCR of 143B-*CYTB*-WT and 143B-*CYTB*-Δ cells ($n = 5$ biologically independent experiments). **b**, Average tumour volume of xenografts from 143B-*CYTB*-WT and 143B-*CYTB*-Δ cells ($n = 10$ mice). **c**, Western blot analysis of QPC in KP-non targeting (NT) and knockout (KO) clones. β-actin was used as a loading control. **d**, Basal OCR of KP-NT and KP-QPC_KO cells ($n = 10$ replicates from two independent experiments). **e**, Luminescence values from the tumours. Values between days 19 and 33 after implantation with KP-NT cells ($n = 7$ mice), or day 33 after implantation with KP-QPC_KO cells ($n = 10$ mice). **f**, Survival of mice implanted with KP-NT ($n = 7$) and QPC_KO cells ($n = 10$). Data are mean ± s.e.m. (**a**, **b**, **e**) or mean ± s.d. (**d**). $^*P < 0.05$, $^{**}P < 0.01$, two-tailed *t*-tests (**a**, **e**), two-way analysis of variance (ANOVA) (**b**) with a Bonferroni test for multiple comparisons, or a one-way ANOVA (**d**) with a Bonferroni test for multiple comparisons (exact *P* values are in the Source Data). Survival curves (**f**) were compared using the log-rank test ($P < 0.0001$). Tumour studies are from two independent cohorts. For gel source data, see Supplementary Fig. 1.

to knock out *Uqcrq*, which encodes the QPC subunit of complex III, in *Kras*$^{G12D/+}$*p53*$^{-/-}$ (KP; *p53* is also known as *Trp53*) cells isolated from mouse lung tumours (Fig. 1c). Loss of QPC in KP cells diminished basal and coupled OCRs (Fig. 1d, Extended Data Fig. 1k), and significantly reduced tumour growth after orthotopic mouse lung transplantation (Fig. 1e). Mice injected with non-targeting KP (KP-NT) cells had significantly worse survival than mice injected with QPC-knockout KP (KP-QPC_KO) cells (Fig. 1f). In addition, we explored the effect of the loss of complex III in T cell acute lymphoblastic leukaemia (T-ALL) in vivo (Extended Data Fig. 2a). Haematopoietic stem cells (HSCs) from donor mice with *loxP*-flanked (*Uqcrq*$^{flox/-}$) or wild-type (*Uqcrq*$^{WT/-}$) *Uqcrc* alleles and tamoxifen-inducible *Ubc-cre*^{ERT2} were transformed and adoptively transferred into immunocompetent mice. After establishment of T-ALL detectable in the peripheral blood of the recipients, tamoxifen was administered to induce the loss (QPC-KO) or maintenance (QPC-WT) of complex III function in T-ALL cells (Extended Data Fig. 2a). Analysis of GFP$^+$ T-ALL cell contents in the spleen and bone marrow revealed that only wild-type QPC cells were able to establish significant T-ALL burden (Extended Data Fig. 2b–e). Accordingly, the spleens of mice containing wild-type QPC T-ALL cells were significantly enlarged compared with those containing knockout QPC (Extended Data Fig. 2f), and mice containing leukaemic cells with functional mitochondria (wild-type QPC) had significantly worse survival (Extended Data Fig. 2g). Collectively, these data indicate that mitochondrial complex III is required for tumour growth in vivo.

Ubiquinol oxidation is an essential activity of mitochondrial complex III that allows complex I, II and DHODH to function. We ectopically and stably expressed GFP or *Ciona intestinalis* AOX in 143B-*CYTB*-Δ cells to restore ubiquinol oxidation[14] (Extended Data Fig. 3a). AOX transports electrons from ubiquinol directly to oxygen, bypassing ETC complex III and IV activities[12]. As a result, AOX restored the basal OCR in 143B-*CYTB*-Δ cells (Fig. 2a). AOX conducts electron flux but not proton pumping, thus it does not directly contribute to the proton-motive force for ATP synthesis. However, ubiquinol oxidation by AOX allows complex I to proton pump, consequently restoring OXPHOS (Extended Data Fig. 3b). AOX expression in 143B-*CYTB*-Δ cells alleviated their auxotrophy for pyruvate and uridine (Fig. 2b), restored the NAD+/NADH ratio (Fig. 2c), aspartate levels (Fig. 2d), and partially rescued TCA cycle metabolite levels in the absence of methyl pyruvate and uridine (Extended Data Fig. 1h). Notably, AOX expression in 143B-*CYTB*-Δ cells rescued tumour growth in vivo (Fig. 2e, Extended Data Fig. 3c). Similarly, AOX expression in KP-QPC_KO cells rescued basal and coupled OCR (Fig. 2f, Extended Data Fig. 3d), and in vivo lung tumour growth (Fig. 2g). Mice transplanted with KP-QPC_KO AOX-expressing cells had significantly worse survival than mice transplanted with KP-QPC_KO GFP-expressing control cells (Fig. 2h). Our results indicate that the essential function of mitochondrial complex III for tumour growth is ubiquinol oxidation and not its ability to proton pump or donate electrons to the downstream electron carrier cytochrome *c*.

Ubiquinol oxidation supports DHODH function (Extended Data Fig. 3a). Similar to the genetic inactivation of cytochrome *b*, treatment with the complex III inhibitor antimycin A rendered 143B-*CYTB*-WT cells auxotrophic for pyruvate and uridine (Extended Data Fig. 3e). However, the complex I inhibitor piericidin A made the cells auxotrophic for pyruvate but not uridine (Extended Data Fig. 3e). Notably, the dihydroorate-to-orotate ratio increased in 143B-*CYTB*-WT cells treated with antimycin A, but not with piericidin A (Extended Data Fig. 3f). These results indicate that the availability of the ubiquinone (Q) pool, which is only compromised when complex III function is inhibited, is the key factor for the maintenance of de novo pyrimidine synthesis. We tested the necessity of the de novo pyrimidine synthesis pathway through CRISPR–Cas9-mediated inactivation of *DHODH* in AOX-expressing 143B-*CYTB*-Δ cells (Extended Data Fig. 4a). Loss of DHODH caused uridine auxotrophy and reduced tumour growth in vivo (Extended Data Fig. 4b–e), and reconstituting its cDNA restored those phenotypes (Extended Data Fig. 4f–i).

Ubiquinol oxidation is required for mitochondrial complex I function. Therefore, we tested the necessity of complex I in AOX-expressing 143B-*CYTB*-Δ cells by inactivating *NDUFS2*, which encodes an essential subunit of complex I (Fig. 3a, Extended Data Fig. 5a). The loss of NDUFS2 made AOX-expressing 143B-*CYTB*-Δ cells auxotrophic for pyruvate in vitro (Fig. 3b), and ablated their in vivo tumour growth (Fig. 3c,

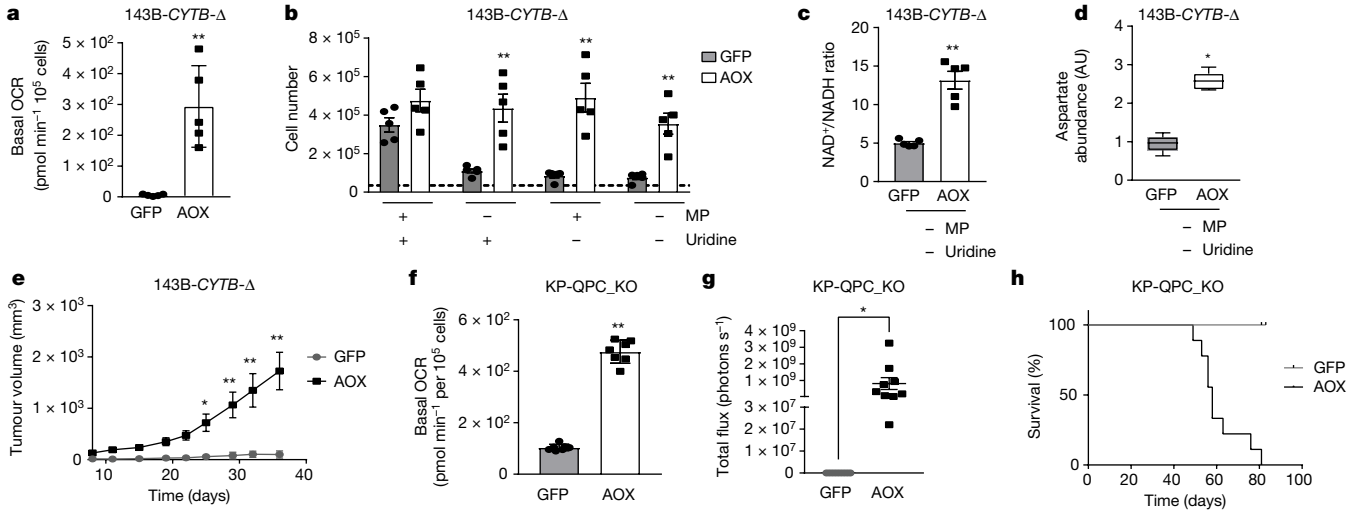

Fig. 2 | Ubiquinol oxidation by complex III is necessary for tumour growth. **a**, Basal OCR of 143B-*CYTB*-Δ-GFP and 143B-*CYTB*-Δ-AOX cells ($n = 5$ biologically independent experiments). **b**, 143B-*CYTB*-Δ-GFP and 143B-*CYTB*-Δ-AOX cells were grown in the presence or absence of methyl pyruvate (MP) and/or uridine, and cell number was assessed after 72 h ($n = 5$ biologically independent experiments). **c**, **d**, Intracellular NAD+/NADH ratio (**c**) and aspartate levels (**d**) of 143B-*CYTB*-Δ-GFP and 143B-*CYTB*-Δ-AOX cells in the absence of methyl pyruvate and uridine ($n = 5$ biologically independent experiments). **e**, Average tumour volume of xenografts from 143B-*CYTB*-Δ-GFP and 143B-*CYTB*-Δ-AOX cells ($n = 9$ mice). **f**, Basal OCR of KP-QPC_KO-GFP and KP-QPC_KO-AOX cells ($n = 7$ technical replicates; representative of five biologically independent experiments). **g**, Luminescence values from the tumours. Values before euthanasia between days 49 and 83 after implantation with KP-QPC_KO-AOX, or day 81 or 83 after implantation with KP-QPC_KO-GFP cells ($n = 9$ mice). **h**, Survival of mice implanted with KP-QPC_KO-GFP and KP-QPC_KO-AOX cells. ($n = 9$ mice). Data are mean ± s.e.m. (**a**–**e**, **g**) or mean ± s.d. (**f**). $^*P < 0.05$, $^{**}P < 0.01$, two-tailed *t*-tests (**a**, **c**, **f**, **g**) or two-way ANOVA (**b**, **e**) with a Bonferroni test for multiple comparisons (exact *P* values are in the Source Data). Survival curves were compared using the log-rank test ($P < 0.0001$). Aspartate levels (**d**) were analysed with multiple one-way ANOVA using a false discovery rate (FDR) value of 0.1 and Fisher's least significant difference test post hoc analyses $Q = 10\%$ ($^*Q < 0.1$; exact *Q* values are in the Source Data). Tumour studies are from two independent cohorts.

Extended Data Fig. 5b). Reconstitution of *NDUFS2* cDNA restored the OCR, pyruvate prototrophy and in vivo tumour growth (Extended Data Fig. 5c–g). Mitochondrial complex I has two key functions: (1) donating electrons from NADH to ubiquinone to result in the generation of NAD+, which allows the oxidative TCA cycle to function, and (2) proton-pumping, which contributes to the generation of ATP

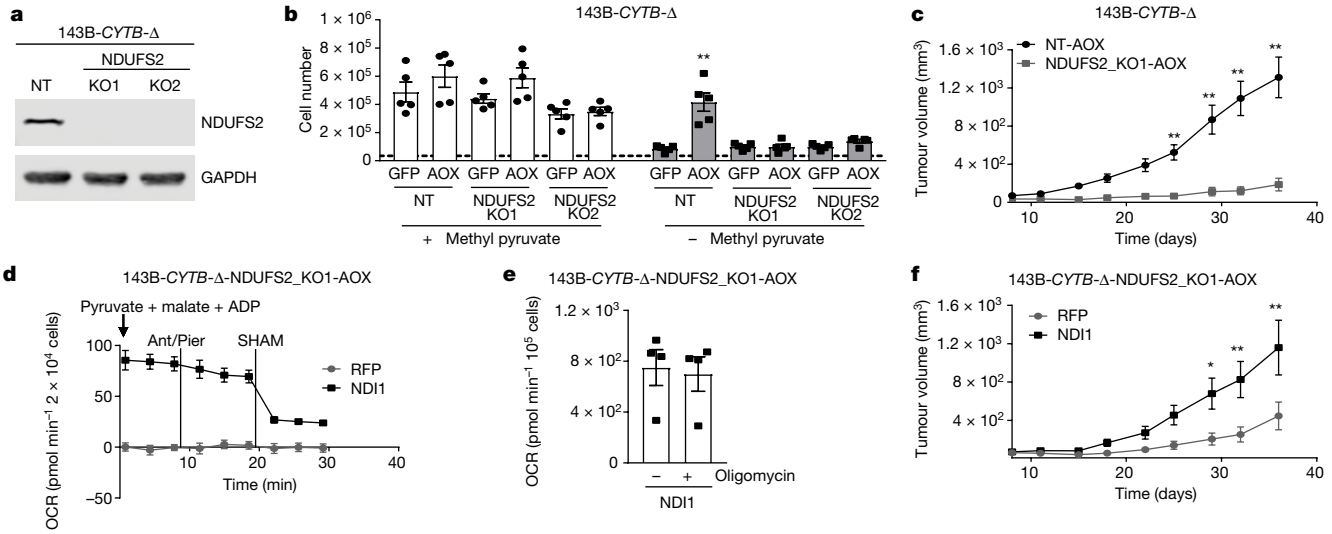

Fig. 3 | Complex I is necessary for tumour growth. **a**, Western blot analysis of NDUFS2 protein levels in 143B-*CYTB*-Δ non-targeting (NT) and 143B-*CYTB*-Δ-NDUFS2_KO cells. GAPDH was used as a loading control. Representative of two independent experiments. **b**, 143B-*CYTB*-Δ-NT and 143B-*CYTB*-Δ-NDUFS2_KO cells expressing either GFP or AOX were grown in medium containing uridine and in the presence or absence of methyl pyruvate, and cell number was assessed after 72 h ($n = 5$ biologically independent experiments). **c**, Average tumour volume of xenografts from 143B-*CYTB*-Δ-NT-AOX and 143B-*CYTB*-Δ-NDUFS2_KO1-AOX cells ($n = 10$ mice). **d**, Complex I-driven OCR of permeabilized 143B-*CYTB*-Δ-NDUFS2_KO1 cells expressing AOX and either RFP or NDI1. Piericidin A (Pier; 1 μM) and antimycin A (Ant; 1 μM) were used to inhibit complex I and III, respectively. Salicylhydroxamic acid (SHAM; 2 mM) was used to inhibit AOX activity ($n = 6$ biologically independent experiments). **e**, OCR in the presence or absence of oligomycin in 143B-*CYTB*-Δ-NDUFS2_KO1 cells expressing AOX and NDI1 ($n = 4$ biologically independent experiments). **f**, Average tumour volume of xenografts from 143B-*CYTB*-Δ-NDUFS2_KO1 cells expressing AOX and either RFP or NDI1 ($n = 10$ mice). Data are mean ± s.e.m. (**b**–**f**). $^*P < 0.05$, $^{**}P < 0.01$, two-tailed *t*-tests (**e**) or two-way ANOVA (**b**, **c**, **f**) with a Bonferroni test for multiple comparisons (exact *P* values are in the Source Data). For gel source data, see Supplementary Fig. 2. Tumour studies are from two independent cohorts.

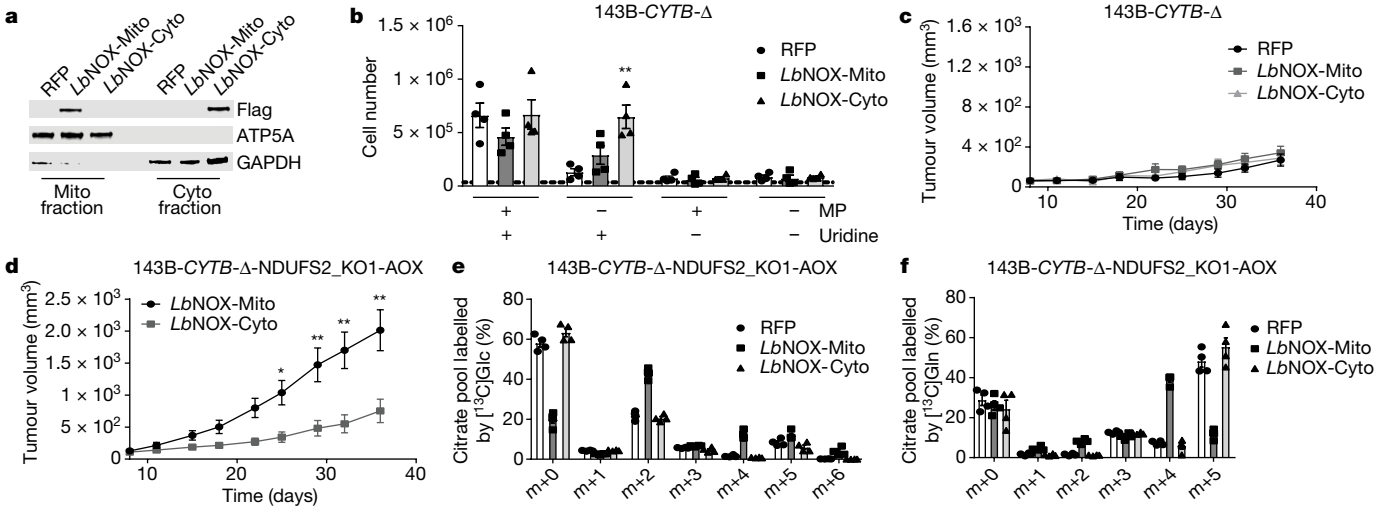

Fig. 4 | Mitochondrial NAD+ regeneration is necessary but not sufficient for tumour growth in vivo. a, Subcellular localization of *Lb*NOX in 143B-*CYTB*-Δ cells determined by cell fractionation. ATP5A is a mitochondrial marker and GAPDH is a cytosolic marker. Representative of three independent experiments. **b**, 143B-*CYTB*-Δ cells expressing mitochondrial (Mito) or cytosolic (Cyto) *Lb*NOX, or red fluorescent protein (RFP) control were grown in the presence or absence of methyl pyruvate and/or uridine, and cell number was assessed after 72 h ($n = 4$ biologically independent experiments). **c**, Average tumour volume of xenografts from 143B-*CYTB*-Δ-RFP, 143B-*CYTB*-Δ-*Lb*NOX-Mito and 143B-*CYTB*-Δ-*Lb*NOX-Cyto cells ($n = 9$ mice). **d**, Average tumour volume of xenografts from 143B-*CYTB*-Δ-NDUFS2_KO1 cells expressing AOX and either mitochondrial or cytosolic *Lb*NOX ($n = 10$ mice). **e**, **f**, 143B-*CYTB*-Δ-NDUFS2_KO1-AOX cells expressing either RFP or *Lb*NOX in mitochondria or cytosol were labelled for 6 h with [U-^{13}C]glucose (**e**) or [U-^{13}C]glutamine (**f**) in the presence of methyl pyruvate, and the percentage of labelled citrate pools was examined. $m + 0$ pools represent unlabelled fractions ($n = 4$ biologically independent experiments). Data are mean ± s.e.m. (**b**–**f**). $^{*}P < 0.05$, $^{**}P < 0.01$, two-way ANOVA (**b**–**d**) with a Bonferroni test for multiple comparisons (exact P values are in the Source Data). For gel source data, see Supplementary Fig. 3. Tumour studies are from two independent cohorts.

through OXPHOS. To investigate whether the proton-pumping activity of complex I is necessary for tumour growth, we ectopically expressed control RFP or the *Saccharomyces cerevisiae* alternative NADH dehydrogenase (NDI1) in the AOX-expressing 143B-*CYTB*-Δ-NDUFS2-knockout (NDUFS2_KO) cells (Extended Data Fig. 6a). NDI1 can oxidize NADH to NAD+ by donating electrons to ubiquinone without generating proton-motive force[14]. Therefore, NDI1 restored mitochondrial NADH oxidation, alleviated pyruvate auxotrophy, and changed the metabolome of the AOX-expressing 143B-*CYTB*-Δ-NDUFS2_KO cells (Fig. 3d, Extended Data Fig. 6b, c). The ETC complex V inhibitor oligomycin did not decrease the OCR, indicating that these cells are unable to conduct OXPHOS (Fig. 3e). Moreover, NDI1-and AOX-expressing 143B-*CYTB*-Δ-NDUFS2_KO cells underwent cell death when glucose was replaced by galactose, which forces cells to rely on mitochondrial ATP for survival (Extended Data Fig. 6d). Notably, NDI1 increased tumour growth of AOX-expressing 143B-*CYTB*-Δ-NDUFS2_KO cells (Fig. 3f, Extended Data Fig. 6e), indicating that OXPHOS is not necessary to support tumour growth.

To test whether mitochondrial NAD+ regeneration is necessary and sufficient for tumour growth, we used the water-forming NADH oxidase from *L. brevis* (*Lb*NOX) targeted to the mitochondrial matrix or cytosol[13]. Expression of the *Lb*NOX increases NAD+/NADH ratios in the respective compartments, and importantly, restores proliferative defects caused by ETC inhibition in vitro[13]. To investigate mitochondrial NAD+ sufficiency for tumour growth, we first expressed the mitochondrial or cytosolic *Lb*NOX in 143B-*CYTB*-Δ cells (Fig. 4a, Extended Data Fig. 7a). Both cytosolic and mitochondrial *Lb*NOX alleviated pyruvate auxotrophy by increasing the NAD+/NADH ratio, levels of TCA cycle metabolites, and cell proliferation in vitro (Fig. 4b, Extended Data Fig. 7b–f). However, neither cytosolic nor mitochondrial *Lb*NOX expression was sufficient to rescue tumour growth in vivo (Fig. 4c, Extended Data Fig. 7g). To further test whether regeneration of NAD+ is necessary for tumour growth, we expressed the mitochondrial or cytosolic *Lb*NOX in AOX-expressing 143B-*CYTB*-Δ NDUFS2-knockout cells (Extended Data Fig. 8a). Expression of either *Lb*NOX relieved the pyruvate auxotrophy of the cells, and increased the NAD+/NADH ratio and aspartate levels of these cells in vitro (Extended Data Fig. 8b–d). Both mitochondrial and cytosolic *Lb*NOX changed the metabolome of the cells in vitro (Extended Data Fig. 6c). Owing to the inability of these cells to perform OXPHOS, cell death was observed when glucose in the growth medium was replaced by galactose (Extended Data Fig. 8e). Notably, only mitochondrial *Lb*NOX supported significant tumour growth in vivo (Fig. 4d, Extended Data Fig. 8f). The expression of both *Lb*NOX oxidases inside the in vivo tumours was confirmed (Extended Data Fig. 8g). A potential difference between cells with mitochondrial versus cytosolic *Lb*NOX is the ability of the former to conduct oxidative TCA metabolism while the latter can only perform reductive TCA metabolism (Extended Data Fig. 9a). It is likely that the oxidative TCA cycle flux generates metabolites more efficiently than reductive TCA cycle flux to support macromolecule synthesis for tumour growth. Indeed, mitochondrial *Lb*NOX supported oxidative TCA cycle flux in the presence of pyruvate, as identified by the increased levels of $m + 2$ and $m + 4$ mass isotopomers of citrate from [U-^{13}C]glucose and [U-^{13}C]glutamine, respectively (Fig. 4e, f). By contrast, cytosolic *Lb*NOX supported reductive metabolism in the presence of pyruvate, as the levels of the $m + 5$ mass isotopomer of citrate, and the $m + 3$ mass isotopomers of fumarate, aspartate and malate from [U-^{13}C]glutamine were significantly increased (Fig. 4f, Extended Data Fig. 9b–d). Notably, the same results were observed in the absence of pyruvate when cells were labelled with [U-^{13}C]glutamine (Extended Data Fig. 9e–h). Collectively, our results indicate that although cytosolic NAD+ regeneration can better rescue the metabolic phenotype of complex I deficient cells in vitro (Extended Data Fig. 6c), mitochondrial NAD+ regeneration, probably owing to its unique ability to restore oxidative TCA cycle flux, is more efficient at supporting tumour growth in vivo. These results further support the limitation of in vitro systems in reflecting the metabolic needs of tumours in vivo.

Oxidation of ubiquinol is also required for mitochondrial complex II function. We tested whether complex II is essential for tumour growth by genetically inactivating *SDHA*, which encodes an essential subunit of complex II, in AOX-expressing 143B-*CYTB*-Δ cells (Extended Data Fig. 10a, b). Previous studies have demonstrated that loss of complex II in cancer cells causes pyruvate auxotrophy for aspartate synthesis[21,22]. Indeed, loss of SDHA in AOX-expressing 143B-*CYTB*-Δ cells diminished complex II activity, induced pyruvate auxotrophy, and suppressed tumour growth in vivo (Extended Data Fig. 10c–f). Reconstitution of SDHA cDNA in the cells rescued those phenotypes (Extended Data Fig. 11a–e). It is important to note that there are rare cancers that exhibit mutations in *SDH* subunits as well as the TCA cycle enzyme fumarate hydratase (*FH*) to generate high levels of succinate and fumarate as oncometabolites[1]. However, these cancer cells are able to conduct reductive TCA cycle metabolism to generate the necessary metabolites for proliferation[1,20–22].

Our results indicate that mitochondrial complex III function is required for tumour growth. Complex III is necessary for ubiquinol oxidation which is essential for complex I and II function and for the de novo pyrimidine synthesis pathway. Our findings indicate that complexes I and II are required for tumour growth owing to the regeneration of mitochondrial NAD+ and FAD, which enable oxidative TCA cycle flux. Cancer cells use various mechanisms including glutaminolysis and autophagy to replenish TCA cycle metabolites[23]. As a result, inhibition of glutaminolysis or autophagy in certain cancers diminishes tumour growth[24,25]. Recently, a study used positron emission tomography (PET) imaging of a radiotracer, 4-[^{18}F]fluorobenzyl triphenylphosphonium (^{18}FBnTP), to non-invasively measure the mitochondrial membrane potential of lung tumours in vivo, which was predictive of their response to complex I inhibitors[26]. In the future, it will be of interest to determine whether complex I inhibitors[27] or mitochondrial TCA cycle inhibitors[28] are efficacious in ongoing phase 3 clinical trials, and to develop safe but potent chemotherapeutic strategies that target mitochondrial metabolism in combination with upcoming technologies that profile the metabolic states of human cancers.

Online content

Any methods, additional references, Nature Research reporting summaries, source data, extended data, supplementary information, acknowledgements, peer review information; details of author contributions and competing interests; and statements of data and code availability are available at https://doi.org/10.1038/s41586-020-2475-6.

1. DeBerardinis, R. J. & Chandel, N. S. We need to talk about the Warburg effect. *Nat. Metab.* **2**, 127–129 (2020).
2. Weinberg, F. et al. Mitochondrial metabolism and ROS generation are essential for Kras-mediated tumorigenicity. *Proc. Natl Acad. Sci. USA* **107**, 8788–8793 (2010).
3. Tan, A. S. et al. Mitochondrial genome acquisition restores respiratory function and tumorigenic potential of cancer cells without mitochondrial DNA. *Cell Metab.* **21**, 81–94 (2015).
4. Ju, Y. S. et al. Origins and functional consequences of somatic mitochondrial DNA mutations in human cancer. *eLife* **3**, (2014).
5. Kuntz, E. M. et al. Targeting mitochondrial oxidative phosphorylation eradicates therapy-resistant chronic myeloid leukemia stem cells. *Nat. Med.* **23**, 1234–1240 (2017).
6. Roth, K. G., Mambetsariev, I., Kulkarni, P. & Salgia, R. The mitochondrion as an emerging therapeutic target in cancer. *Trends Mol. Med.* **26**, 119–134 (2020).
7. Navarro, P. et al. Targeting tumor mitochondrial metabolism overcomes resistance to antiangiogenics. *Cell Rep.* **15**, 2705–2718 (2016).
8. Kim, S. H. et al. Phenformin inhibits myeloid-derived suppressor cells and enhances the anti-tumor activity of PD-1 blockade in melanoma. *J. Invest. Dermatol.* **137**, 1740–1748 (2017).
9. Viale, A. et al. Oncogene ablation-resistant pancreatic cancer cells depend on mitochondrial function. *Nature* **514**, 628–632 (2014).
10. Maher, E. A. et al. Metabolism of [U-^{13}C]glucose in human brain tumors in vivo. *NMR Biomed.* **25**, 1234–1244 (2012).
11. Hensley, C. T. et al. Metabolic heterogeneity in human lung tumors. *Cell* **164**, 681–694 (2016).
12. Hakkaart, G. A., Dassa, E. P., Jacobs, H. T. & Rustin, P. Allotopic expression of a mitochondrial alternative oxidase confers cyanide resistance to human cell respiration. *EMBO Rep.* **7**, 341–345 (2006).
13. Titov, D. V. et al. Complementation of mitochondrial electron transport chain by manipulation of the NAD+/NADH ratio. *Science* **352**, 231–235 (2016).
14. Martínez-Reyes, I. et al. TCA cycle and mitochondrial membrane potential are necessary for diverse biological functions. *Mol. Cell* **61**, 199–209 (2016).
15. Garcia-Bermudez, J. et al. Aspartate is a limiting metabolite for cancer cell proliferation under hypoxia and in tumours. *Nat. Cell Biol.* **20**, 775–781 (2018).
16. Sullivan, L. B. et al. Supporting aspartate biosynthesis is an essential function of respiration in proliferating cells. *Cell* **162**, 552–563 (2015).
17. Sullivan, L. B. et al. Aspartate is an endogenous metabolic limitation for tumour growth. *Nat. Cell Biol.* **20**, 782–788 (2018).
18. Birsoy, K. et al. An essential role of the mitochondrial electron transport chain in cell proliferation is to enable aspartate synthesis. *Cell* **162**, 540–551 (2015).
19. Bajzikova, M. et al. Reactivation of dihydroorotate dehydrogenase-driven pyrimidine biosynthesis restores tumor growth of respiration-deficient cancer cells. *Cell Metab.* **29**, 399–416 (2019).
20. Mullen, A. R. et al. Reductive carboxylation supports growth in tumour cells with defective mitochondria. *Nature* **481**, 385–388 (2011).
21. Lussey-Lepoutre, C. et al. Loss of succinate dehydrogenase activity results in dependency on pyruvate carboxylation for cellular anabolism. *Nat. Commun.* **6**, 8784 (2015).
22. Cardaci, S. et al. Pyruvate carboxylation enables growth of SDH-deficient cells by supporting aspartate biosynthesis. *Nat. Cell Biol.* **17**, 1317–1326 (2015).
23. DeBerardinis, R. J. & Chandel, N. S. Fundamentals of cancer metabolism. *Sci. Adv.* **2**, e1600200 (2016).
24. Guo, J. Y. et al. Activated Ras requires autophagy to maintain oxidative metabolism and tumorigenesis. *Genes Dev.* **25**, 460–470 (2011).
25. Romero, R. et al. Keap1 loss promotes Kras-driven lung cancer and results in dependence on glutaminolysis. *Nat. Med.* **23**, 1362–1368 (2017).
26. Momcilovic, M. et al. In vivo imaging of mitochondrial membrane potential in non-small-cell lung cancer. *Nature* **575**, 380–384 (2019).
27. Molina, J. R. et al. An inhibitor of oxidative phosphorylation exploits cancer vulnerability. *Nat. Med.* **24**, 1036–1046 (2018).
28. Alistar, A. et al. Safety and tolerability of the first-in-class agent CPI-613 in combination with modified FOLFIRINOX in patients with metastatic pancreatic cancer: a single-centre, open-label, dose-escalation, phase 1 trial. *Lancet Oncol.* **18**, 770–778 (2017).

Methods

Cell culture and drug treatment

143B-*CYTB*-WT and 143B-*CYTB*-Δ cells were previously described[2]. Mouse *Kras*$^{G12D/+}$*p53*$^{-/-}$ (KP) lung tumour cells expressing luciferase were generously provided by T. Papagiannakopoulos. Cells were grown in DMEM containing 4.5 g l^{-1} glucose, 4 mM L-glutamine (Gibco; 11965-126) supplemented with 10% Nu-serum IV (Corning), 1 mM methyl pyruvate, 400 μM uridine, 1% HEPES and 1% antibiotic-antimycotic (Gibco) at 37 °C with 5% CO_2. Hygromycin (600 μg ml^{-1}) was used to select luciferase expressing KP cells. 143B-*CYTB*-WT were treated with: 500 nM antimycin A (Sigma) and 500 nM piericidin A (Sigma). pWPI-EF1-GFP vectors with AOX and NDI1 were a gift from E. Dufour. The full-length coding sequences of *N*DI1, NDUFS2, SDHA, DHODH, *Lb*NOX-Mito (Addgene; 74448; V. Mootha laboratory), and *Lb*NOX-Cyto (Addgene; 75285; V. Mootha laboratory) were subcloned into the pLV-EF1-RFP vector (VectorBuilder). The resultant NDI1, NDUFS2, SDHA, DHODH, *Lb*NOX-Mito and *Lb*NOX-Cyto vectors, as well as their empty vector control, pLV-EF1-RFP, were transfected into 293T cells (ATTC) along with pMD2.G and psPAX2 packaging vectors using jetPRIME transfection reagent (Polyplus) to produce control-RFP, NDI1-RFP, NDUFS2-RFP, SDHA-RFP, DHODH-RFP, *Lb*NOX-Mito-RFP and *Lb*NOX-Cyto-RFP lentivirus. Similarly, AOX vector and its empty vector control, pWPI-EF1-GFP, were transfected into 293T to generate control-GFP and AOX-GFP lentivirus. Three days after transduction with the indicated virus, GFP- or RFP-positive cells were sorted using a BD FACSAria cell sorter. The cells were periodically sorted to maintain high levels of protein expressions. To generate 143B-*CYTB*-Δ-NDUFS2_KO, 143B-*CYTB*-Δ-SDHA_KO, 143B-*CYTB*-Δ-DHODH_KO and KP-QPC_KO cell lines, gene-specific single-guides RNAs (sgRNAs) listed in Supplementary Table 1 were cloned into the pSpCas9(BB)-2A-GFP (PX458) plasmid (Addgene; 48138; F. Zhang laboratory). These sgRNA-Cas9-GFP vectors were transfected into 143B-*CYTB*-Δ or KP cells using the jetPRIME (Polyplus). Two days after transfection, the GFP-positive cells were single-cell sorted into a 96-well plate using a BD FACSAria cell sorter. The cells were grown for 2–3 weeks, and the resultant clonal cell lines were expanded. Immunoblotting was used to confirm knockout of the targeted gene. Cells have not been authenticated. Cells tested negative for mycoplasma contamination.

Cellular fractionation and immunoblot analysis

Mitochondria were isolated with the human mitochondria isolation kit (Miltenyi Biotec) using 7×10^6–9×10^6 cells, following the manufacturer's instructions. Purified mitochondria were then lysed using the 1× cell lysis buffer (Cell Signaling) containing the Halt protease inhibitor cocktail (Thermo Scientific). The cytosolic fraction was prepared by differential centrifugation using cells from one 10 cm dish. Cells were resuspended in 0.5 ml of PBS with the Halt protease inhibitor cocktail, and lysed by passing through a 27.5-guage needle 12 times. Intact cells and nuclei were removed by centrifugation for 10 min at 800*g* at 4 °C. The supernatant was transferred to a new Eppendorf tube and centrifuged for 10 min at 8,000*g* at 4 °C. The resultant supernatant was the cytosolic fraction. Whole-cell lysate extracts were prepared from the indicated cell lines by collecting and lysing cells in 1× cell lysis buffer containing the Halt protease inhibitor cocktail. The Pierce BCA Protein Assay kit (Thermo Scientific) was used to quantify the protein concentrations. Approximately 50–100 μg of lysate was resolved on a SDS–PAGE gel (Bio-Rad) and transferred to a nitrocellulose membrane using the Trans-Blot Turbo Transfer System (Bio-Rad). Membranes were first blocked in 5% milk for 1 h, then incubated in the primary antibody overnight. Primary antibodies used were: anti-NDUFS2 (Abcam; ab103024; 1:500 dilution), anti-QPC (Abcam; ab136679; 1:500 dilution), anti-SDHA (MitoScience; MS204; clone 2E3GC12FB2AE2; 1:500 dilution), anti-DHODH (Santa Cruz; sc-166348; clone E-8; 1:500 dilution), anti-FLAG (Sigma; F1804; clone M2; 1:1,000 dilution), anti-GAPDH (Santa Cruz; sc-32233; clone 6C5, and Sigma; G9545; 1:2,000 dilution), anti-ATP5A (Mitosciences; MS507; clone 15H4C4; 1:1,000 dilution), anti-tubulin (Cell Signaling; 2144; 1:1,000 dilution) and anti-β-actin (Sigma; A2228-100UL; clone AC-74,). IRDye 800CW goat anti-rabbit (LI-COR; 926-32211) and IRDye 680RD goat anti-mouse (LI-COR; 926-68070) were used as secondary antibodies. Image Studio Lite version 3.1 (LI-COR) was used for the analysis of protein levels.

Mouse models and tumour studies

Uqcrq (QPC) floxed (flox), wild-type (WT) and null (−) alleles were genotyped using the following primers: QPC-F- CTTCCGCTCCTCCCGGAAGT; QPC-R- TTCCCAAACTCGCGGCCCATG and QPC-null- CAATTCCAGCCAACAGTCCC. *Ubc-cre*^{ERT2} mice were obtained from the Jackson Laboratory. *Uqcrq*$^{flox/flox}$, *Uqcrq*$^{WT/-}$ and *Ubc-cre*^{ERT2} mice were crossed to generate T-ALL donors containing *Ubc-cre*^{ERT2} alleles with floxed/null *Uqcrq* (*Uqcrq*$^{flox/-}$*;Ubc-cre*^{ERT2}), or wild-type/null *Uqcrq* (*Uqcrq*$^{WT/-}$*; Ubc-cre*^{ERT2}) as control. Mice of both sexes aged 8–12 weeks old were used for experiments. Mice were not randomized to experimental groups, but were age-matched, sex-matched, and littermates when possible. For xenograft tumour studies, 4×10^6 cells were subcutaneously injected into male J:Nu mice (8–12 weeks). Tumours were measured twice a week and tumour volume was calculated using the following equation: $(4/3) \times \pi \times$ (arithmetic mean of 2 calliper measurements)/2)^3. At the completion of the study, mice were euthanized and the tumours were extracted and weighed. Mice were euthanized before the endpoint was reached if tumours reached 2 cm diameter, developed ulcerations or mice exhibited distress. For the orthotopic lung tumour model, 2.5×10^5 KP cells in 50–75 μl of PBS plus 2.5mM EDTA were intratracheally instilled in C57BL/6J mice as previously described[29]. In vivo luciferase was imaged on IVIS or LAGO system to monitor tumour growth. The fur on the chest was first removed using Nair hair removal cream. Subsequently, 150 μl of RediJect D-Luciferin Ultra Bioluminescent Substrate (PerkinElmer) was injected inraperitoneally, and images were taken after 10 min. Images were processed using the Living Image or Aura software to measure the background-corrected bioluminescence signal from the tumours. Mice were euthanized by 20 weeks after tumour administration, or after losing 15–20% initial weight or displaying overt distress. All mice were housed in the Northwestern University animal vivarium and we have complied with all relevant ethical regulations in accordance with Northwestern University Institutional Animal Care and Use Committee (IACUC).

Bone marrow isolation and leukaemic transformation

Platinum-E retroviral packaging cells and MIGR1-Notch1$^{\Delta E}$-GFP vector were a gift from P. Ntziachristos. Platinum-E cells were transfected with MIGR1-Notch1$^{\Delta E}$-GFP plasmid using jetPRIME (Polyplus) in order to generate the Notch1$^{\Delta E}$-GFP retrovirus. Bone marrow cells were obtained from *Uqcrq*$^{flox/-}$*;Ubc-cre*^{ERT2} and *Uqcrq*$^{WT/-}$*;Ubc-cre*^{ERT2} donor mice by grinding the pelvis, femur and tibia bones with a mortar and a pestle. From the bone marrow cells, HSCs were isolated by a CD117$^+$ positive selection magnetic bead isolation kit (StemCell). Subsequently, HSCs were transduced with the Notch1$^{\Delta E}$-GFP retrovirus by centrifugation at 25 °C at 1,500*g* for 90 min, followed by incubation in 37 °C overnight. The virus was removed the next day morning, after which cells were allowed to rest for 2 days. The transduction and culturing of HSCs were performed in Opti-MEM (Thermo Fisher) supplemented with 10 ng ml^{-1} IL-3 (PeproTech), 10 ng ml^{-1} IL-7 (PeproTech), 50 ng ml^{-1} SCF (PeproTech), 50 ng ml^{-1} FLT3L (PeproTech), and 20 ng ml^{-1} IL-6 (PeproTech). Approximately 24 h before adoptive transfer, wild-type C57BL/6J recipients were lethally irradiated at approximately 1,000 rad. On the day of the transfer, lineage (CD4, CD8a, B220, CD11b, Gr-1, NK1.1, Ter-119)-negative and GFP-positive cells were sorted on BD FACS Aria systems. Antibodies used were: anti-Mouse Ter-119 (eBioscience; 48-5921-80; clone TER-119), anti-Mouse NK1.1 (eBioscience; 48-5941-80; clone PK136,), anti-Human/Mouse CD45R (B220) (eBioscience;

48-0452-80; clone RA3-6B2), anti-Mouse CD8a (eBioscience; #48-0081-82; clone 53-6.7), anti-Mouse CD11b (eBioscience; 48-0112-80; clone M1/70,), anti-Mouse Ly-6G (Gr-1) (eBioscience; 48-5931-80; clone RB6-8C5), anti-Mouse CD4 (Tonbo Biosciences; 75-0041-U100; clone GK1.5). Approximately 50,000–100,000 GFP-positive HSCs, along with 500,000 support bone marrow cells isolated from wild-type C57BL/6J mice, were injected intravenously into the recipient mice. At 3 and 4 weeks after transfer, peripheral blood from the recipients was analysed to assess the presence of circulating GFP-positive T-ALL cells. Once the percentage of GFP-positive cells in the peripheral blood reached approximately 5–10%, the recipients were oral gavaged with 320 mg kg^{-1} tamoxifen suspended in corn oil four times, once every 2 days. For up to 25 weeks after tamoxifen administration, the recipients were closely monitored for any signs of malignancy, including weight loss, hunched posture and lethargy. The recipients were euthanized upon displaying 15–20% weight loss, or at up to 30 weeks after transfer. Cell from spleen and bone marrow (from one set of pelvis, femur and tibia) were obtained from each recipient, and stained with Ghost Dye Red 780 (Tonbo Bioscience). The cells were resuspended in FACS buffer (DPBS with 10% NuSerum IV) with PKH reference microbeads (Sigma). The number and the percentage of GFP-positive T-ALL cells were analysed on BD FACSymphony and FlowJo software version 10.4.2.

Proliferation and cell viability analysis

Approximately 3.5×10^4 cells were plated on 6-well plates. Cells were expanded in the presence or absence of methyl pyruvate and/or uridine for 72 h. To assess proliferation, cells were counted using AccuCount Fluorescent Particles (Spherotech) by flow cytometry. Cell viability was determined by measuring the percentage DAPI-positive population by flow cytometry. All flow cytometry assays were performed on BD FACSymphony or BD Fortessa analysers, and data were analysed with the FlowJo software 10.4.2.

Mitochondrial activity studies

The OCR was measured in a XF96 extracellular flux analyser (Seahorse Bioscience). Basal mitochondrial respiration was assessed by subtracting the non-mitochondrial OCR, measured with 1 µM antimycin A and 1 µM piericidin A, from baseline OCR. Coupled respiration was determined by subtracting the OCR in the presence of 1 µM oligomycin A (Sigma) from the basal mitochondrial respiration. To determine mitochondrial complex I activity, growth medium was replaced with mitochondrial assay buffer (70 mM sucrose, 220 mM mannitol, 10 mM KH_2PO_4, 5 mM $MgCl_2$, 2 mM HEPES, 1 mM EGTA, 0.2% (w/v) fatty acid-free BSA, pH 7.2) supplemented with 1 nM Seahorse XF plasma membrane permeabilizer and 10 mM ADP, as well as 2.5 mM malate and 10 mM pyruvate (complex I substrates). To assess mitochondrial complex II activity, growth medium was replaced with the mitochondrial assay buffer containing membrane permeabilizer and ADP, along with 10 mM succinate (complex II substrate) and 1 µM piericidin A, which inhibits the complex I contribution to OCR. The increase in OCR was measured immediately after addition of substrates. Where indicated, Piericidin A and Antimycin A were injected to inhibit complex I and III, respectively. Salicylhydroxamic acid (SHAM; Sigma), was injected to inhibit AOX.

Metabolomics

Subconfluent culture dishes were incubated for 2, 8 or 24 h in DMEM (Gibco; A1443001) supplemented with 15 mM glucose, 2 mM glutamine and 10% dialysed FBS (PEAK Serum), in the presence or absence of 1 mM methyl pyruvate and/or 400 µM uridine. Following the incubation, cells were washed with ice-cold 0.9% NaCl, and overlaid with ultra-cold HPLC grade-methanol/water (80/20, v/v). The plates were incubated at −80 °C for 20 min, after which cells were scraped and collected. The cell suspensions were then centrifuged at 16,000*g* for 15 min at 4 °C. The supernatant was transferred to a new tube and evaporated to dryness using a SpeedVac concentrator (Thermo Savant). Metabolites were reconstituted in 50% acetonitrile in analytical-grade water, vortex-mixed, and centrifuged to remove debris. Samples were analysed by high-performance liquid chromatography and high-resolution mass spectrometry and tandem mass spectrometry (HPLC–MS/MS). Specifically, system consisted of a Thermo Q-Exactive in line with an electrospray source and an Ultimate3000 (Thermo) series HPLC consisting of a binary pump, degasser, and auto-sampler outfitted with a Xbridge Amide column (Waters; dimensions of 4.6 mm × 100 mm and a 3.5 µm particle size). Mobile phase A contained 95% (v/v) water, 5% (v/v) acetonitrile, 10 mM ammonium hydroxide, 10 mM ammonium acetate, pH 9.0; and mobile phase B was 100% acetonitrile. The gradient was as follows: 0 min, 15% A; 2.5 min, 30% A; 7 min, 43% A; 16 min, 62% A; 16.1–18 min, 75% A; 18–25 min, 15% A with a flow rate of 400 µl min^{-1}. The capillary of the ESI source was set to 275 °C, with sheath gas at 45 arbitrary units, auxiliary gas at 5 arbitrary units and the spray voltage at 4.0 kV. In positive/negative polarity switching mode, an m/z scan range from 70 to 850 was chosen and MS1 data were collected at a resolution of 70,000. The automatic gain control (AGC) target was set at 1×10^6 and the maximum injection time was 200 ms. The top five precursor ions were subsequently fragmented, in a data-dependent manner, using the higher energy collisional dissociation (HCD) cell set to 30% normalized collision energy in MS2 at a resolution power of 17,500. Sample volumes of 10 µl were injected. Data acquisition and analysis were carried out by Xcalibur 4.1 software and Tracefinder 4.1 software, respectively (both from Thermo Fisher Scientific). The peak area for each detected metabolite was normalized by the total ion current, which was determined by integration of all of the recorded or annotated peaks within the acquisition window. For carbon labelling, isotopic labelling was performed in DMEM (Gibco; A1443001) supplemented with 10% dialysed FBS, and 2 mM L-[U-^{13}C]glutamine or 10 mM D-[U-^{13}C]glucose, in the presence or absence of 1 mM methyl pyruvate. After 6 h of labelling, metabolites were extracted with ultra-cold HPLC grade-methanol/water (80/20, v/v) and analysed as previously described[20]. Metabolite analyses were carried out in MetaboAnalyst 4.0. Peak intensities normalized to total ion current in tables were loaded. Missing and 0 values were replaced with half the minimum positive values in the original data assuming to be the detection limit. For heat maps with two groups, *t*-tests with an FDR cut-off value of 0.1 were used to identify significantly changed metabolites. For heat maps with more than two groups, one-way ANOVA with Fisher's least significant difference post hoc analyses and an FDR cut-off value of 0.1 was used to generate a list of significantly changed metabolites among groups. This list was then plotted as a heat map with euclidean distance measures and ward.D clustering algorithm of metabolites/rows. Within row, *z*-scores for each metabolite were plotted.

Measurement of dihydroorotate and orotate ratio

For the measurement of dihydroorotate and orotate, 5×10^6 cells were seeded in a 100 mm cell culture dish, and incubated with DMEM (Gibco; A1443001) supplemented with 15 mM glucose, 2 mM glutamine, 10% dialysed FBS, 1% HEPES and 1% antibiotic-antimycotic. After 24 h, metabolites were extracted. Cells were washed twice with DPBS, and lysed with 600 µl of HPLC grade-methanol/chloroform (67/33, v/v). The cell lysates were collected, vortexed for 30 s, and incubated in liquid nitrogen for 60 s. Samples were then thawed at room temperature, after which 400 µl of a HPLC grade-chloroform/water (50/50, v/v) was added. The lysates with metabolites were centrifuged at 15,000*g* for 30 min at 4 °C. The supernatant was transferred to a new tube and evaporated to dryness using a SpeedVac concentrator (Thermo Savant). Samples were analysed by HPLC–MS/MS as described above using targeted selected ion monitoring (tSIM) mode.

Statistical analysis

P values were calculated as described in each figure legend using Graphpad Prism 7 (Graphpad Software) and MetaboAnalyst 4.0[30]. Data are

presented as mean ± s.e.m. unless stated otherwise. Numbers of biological replicates are indicated in the figure legends. The investigators were not blinded during experiments and outcome assessments. No statistical method was used to predetermine sample size, and experiments were not randomized.

Reporting summary

Further information on research design is available in the Nature Research Reporting Summary linked to this paper.

Data availability

All data from the manuscript are available from the corresponding author on request. Source data are provided with this paper.

29. DuPage, M., Dooley, A. L. & Jacks, T. Conditional mouse lung cancer models using adenoviral or lentiviral delivery of Cre recombinase. *Nat. Protoc.* **4**, 1064–1072 (2009).
30. Chong, J. et al. MetaboAnalyst 4.0: towards more transparent and integrative metabolomics analysis. *Nucleic Acids Res.* **46** (W1), W486–W494 (2018).

Acknowledgements This work was supported by the NIH (5R35CA197532) to N.S.C.; a postdoctoral fellowship by Ramon Areces Foundation of Spain to I.M.R.; NCI (T32 CA009560) and NIH (2T32HL076139-16) to H. Kong; NIH (5 T32 CA 9560-33) and Northwestern University Pulmonary department's Cugell fellowship to K.V.; NIH (T32CA09560 and T32HL076139-13) to G.S.M., and NIH (T32 T32HL076139) to S.E.W. E.M.S. is a Cancer Research Institute Irvington Fellow supported by the Cancer Research Institute. We thank Robert H. Lurie Cancer Center Flow Cytometry facility supported by NCI CCSG P30 CA060553 for their invaluable assistance. Imaging work was performed at the Northwestern University Center for Advanced Microscopy generously supported by NCI CCSG P30 CA060553 awarded to the Robert H Lurie Comprehensive Cancer Center. We thank T. Papagiannakopoulos and S. Leboeuf for providing KP cells. We thank C. Moraes for *CYTB*-Δ cells. Original *Lb*NOX constructs were generated by V. Mootha's laboratory and acquired from Addgene. We thank E. Dufour and H. Jacobs for original NDI1 and AOX constructs. We thank P. Ntziachristos for the MIGR1-Notch1$^{\Delta E}$-GFP vector. We thank the members of the Chandel laboratory for discussions.

Author contributions I.M.-R. and N.S.C. conceptualized the study, interpreted the data, and wrote the manuscript with the input of co-authors. I.M.-R., L.R.C., H. Kong, M.W., H. Kihshen, G.S.M., C.R.R. and K.V. carried out most of the experiments in the paper. I.M.-R., L.R.C. and H. Kong performed leukaemia experiments. I.M.-R., L.R.C., H. Kong and K.V. performed lung tumour experiments. I.M.-R., L.R.C., C.R.R, G.S.M. and S.E.W. carried out xenograft experiments. I.M.-R., M.W. and H. Kihshen performed experiments to analyse the OCR in intact and permeabilized cells. I.M.-R., C.R.R. and M.W performed experiments to assess proliferation. I.M.-R. and M.W. performed western blot experiments. I.M.-R., L.R.C., G.S.M. and P.G. conducted and analysed metabolomics and carbon flux experiments. R.P., G.R.S.B., E.M.S. and S.E.W. provided technical expertise with mouse experiments.

Competing interests N.S.C. is a scientific advisory board member of Rafael Pharmaceuticals.

Additional information

Supplementary information is available for this paper at https://doi.org/10.1038/s41586-020-2475-6.

Correspondence and requests for materials should be addressed to N.S.C.

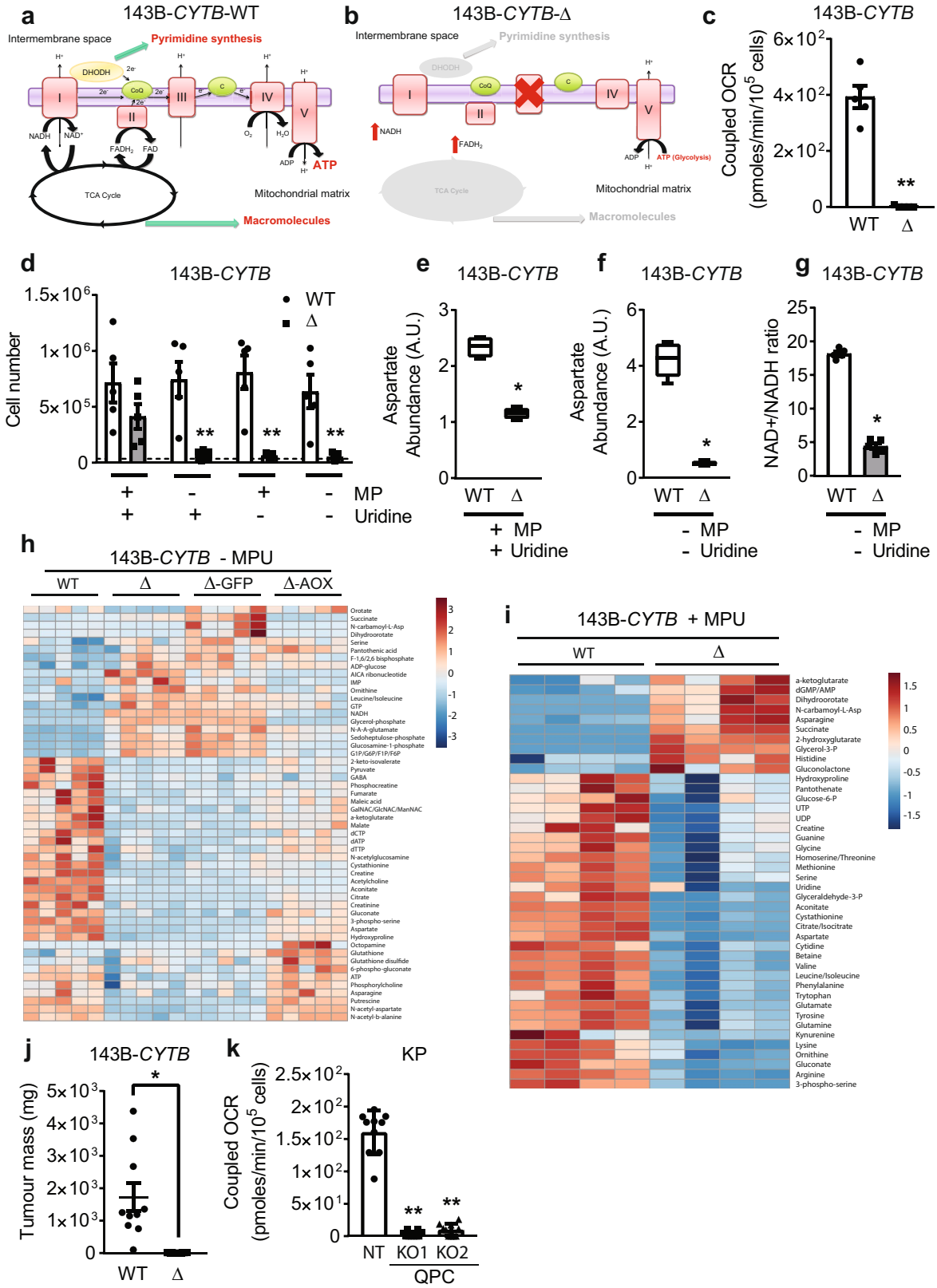

Extended Data Fig. 1 | See next page for caption.

Extended Data Fig. 1 | Metabolite changes in complex III deficient cells in the presence or absence of pyruvate and uridine. a, **b**, Schematic representation of the ETC in 143B-*CYTB*-WT (**a**) and 143B-*CYTB*-Δ cells (**b**). **c**, Coupled OCR of 143B-*CYTB*-WT and 143B-*CYTB*-Δ cells ($n = 5$ biologically independent experiments). **d**, 143B-*CYTB*-WT and 143B-*CYTB*-Δ cells were grown in the presence or absence of methyl pyruvate and/or uridine and cell number was assessed after 72 h ($n = 5$ biologically independent experiments). **e**, Intracellular aspartate levels in the presence of methyl pyruvate and uridine in 143B-*CYTB*-WT and 143B-*CYTB*-Δ cells ($n = 4$ biologically independent experiments). **f**, Intracellular aspartate levels in the absence of methyl pyruvate and uridine in 143B-*CYTB*-WT and 143B-*CYTB*-Δ cells ($n = 5$ biologically independent experiments). **g**, Intracellular NAD+/NADH ratio in the absence of methyl pyruvate and uridine of 143B-*CYTB*-WT and 143B-*CYTB*-Δ cells ($n = 5$ biologically independent experiments). **h**, The heat map displays the relative abundance of significantly changed metabolites in 143B-*CYTB*-WT, 143B-*CYTB*-Δ cells and in 143B-*CYTB*-Δ cells expressing either GFP or AOX in the absence of methyl pyruvate and uridine. A red–blue colour scale depicts the abundance of the metabolites (red: high, blue: low) ($n = 5$ biologically independent experiments). **i**, The heat map displays the relative abundance of significantly changed metabolites in 143B-*CYTB*-WT and 143B-*CYTB*-Δ cells in the presence of methyl pyruvate and uridine ($n = 4$ biologically independent experiments). **j**, Tumour mass of xenografts from 143B-*CYTB*-WT and 143B-*CYTB*-Δ cells ($n = 10$ mice per group from two independent cohorts). **k**, Coupled OCR of KP-NT and KP-QPC_KO cells ($n = 10$ technical replicates from two independent experiments). Data are mean ± s.e.m. (**c**–**g**, **j**) or mean ± s.d. (**k**). $^{*}P < 0.05$, $^{**}P < 0.01$, two-tailed *t*-tests (**c**, **g**, **j**), two-way ANOVA (**d**) with a Bonferroni test for multiple comparisons or one-way ANOVA (**k**) with a Bonferroni test for multiple comparisons (exact *P* values are in the Source Data). Metabolites levels were analysed with multiple one-way ANOVA using an FDR of 0.1 and Fisher's least significant difference test post hoc analyses $Q = 10\%$. For two-group heat maps, *t*-tests with an FDR cut-off value of 0.1 were used to identify significantly changed metabolites. Each row was analysed individually. ($^{*}Q < 0.1$; exact *Q* values are in the Source Data).

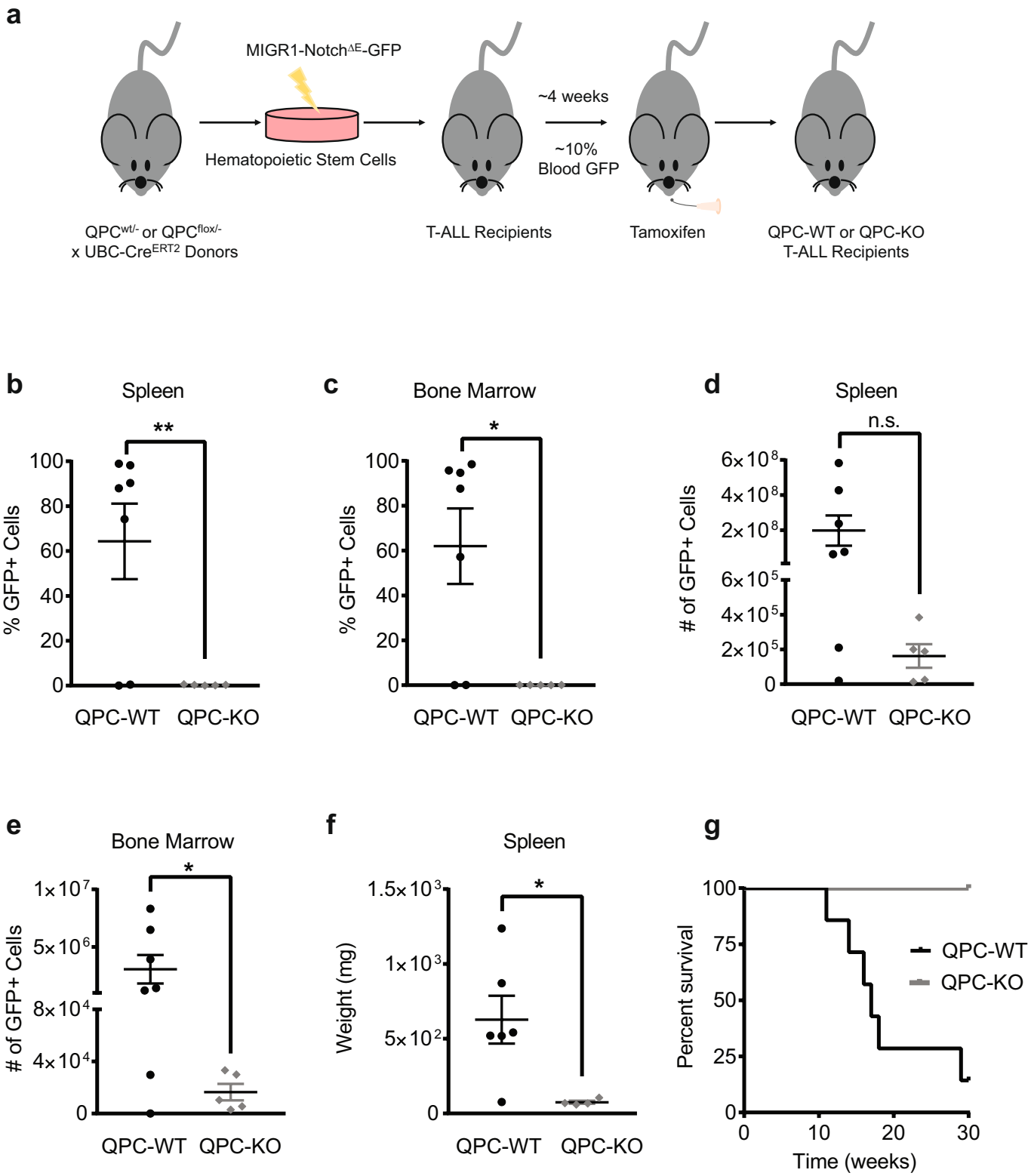

Extended Data Fig. 2 | Mitochondrial complex III is required for T-ALL growth in vivo. a, Schematic representation of the T-ALL experiments. **b**, **c**, Percentage of GFP$^+$ T-ALL cells from the spleen (**b**) or bone marrow (**c**) of QPC-WT and QPC-KO recipients (WT: $n = 7$; KO: $n = 5$ mice). **d**, **e**, The absolute number of GFP$^+$ T-ALL cells from the spleen (**d**) or bone marrow (**e**) of QPC-WT and QPC-KO recipients (WT: $n = 7$; KO: $n = 5$ mice). **f**, Weight of spleens from QPC-WT and QPC-KO recipients (WT: $n = 6$; KO: $n = 4$ mice). **g**, Survival of mice injected with QPC-WT or QPC-KO T-ALL cells (WT: $n = 7$; KO: $n = 4$ mice). Data are mean ± s.e.m. from three independent experiments. $^*P < 0.05$, $^{**}P < 0.01$, two-tailed *t*-tests with a Welch's correction (exact *P* values are in the Source Data). Survival curves were compared using the log-rank test ($P < 0.0001$). An example of the gating strategy is provided in Supplementary Fig. 7.

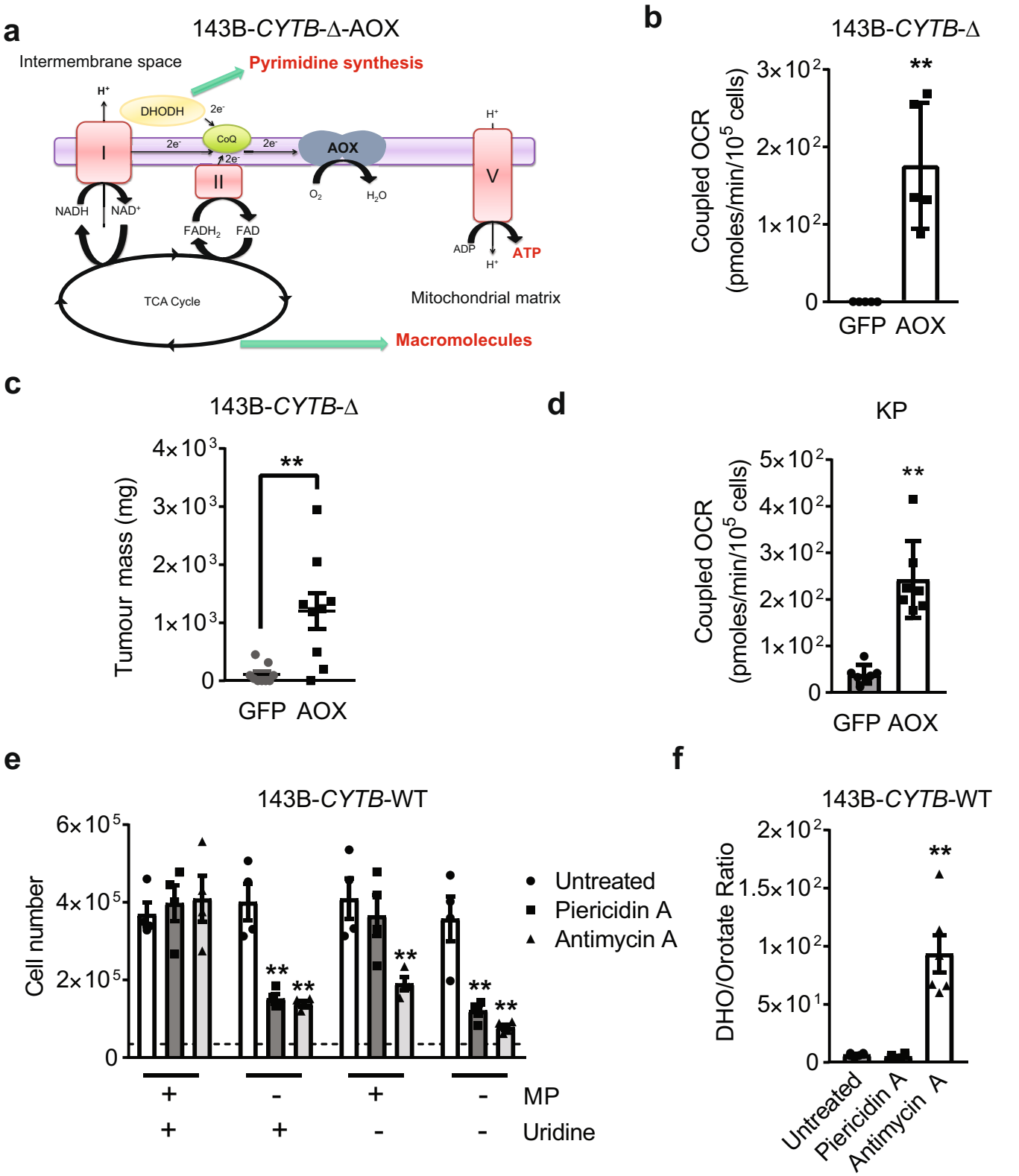

Extended Data Fig. 3 | Complex III-deficient cells are auxotrophic for uridine. a, Schematic representation of the ETC in AOX expressing 143B-*CYTB*-Δ cells. **b**, Coupled OCR of 143B-*CYTB*-Δ-GFP and 143B-*CYTB*-Δ-AOX cells ($n = 5$ biologically independent experiments). **c**, Tumour mass of xenografts from 143B-*CYTB*-Δ-GFP and 143B-*CYTB*-Δ-AOX cells ($n = 9$ mice per group from two independent cohorts). **d**, Coupled OCR of KP-QPC_KO-GFP and KP-QPC_KO-AOX cells ($n = 7$ replicates from one representative of five biologically independent experiments). **e**, 143B-*CYTB*-WT treated or untreated with piericidin A (0.5 µM) or antimycin A (0.5 µM) were grown in the presence or absence of methyl pyruvate and/or uridine and cell number was assessed after 72 h ($n = 4$ biologically independent experiments). **f**, The dihydroorotate-to-orotate ratio was assessed in 143B-*CYTB*-WT treated or untreated with piericidin A (0.5 µM) or antimycin A (0.5 µM) ($n = 6$ biologically independent experiments). Data are mean ± s.e.m. (**b**, **c**, **e**, **f**) or mean ± s.d. (**d**). $^*P < 0.05$, $^{**}P < 0.01$, two-tailed *t*-tests (**b**–**d**), two-way ANOVA (**e**) with a Bonferroni test for multiple comparisons or one-way ANOVA (**f**) with a Bonferroni test for multiple comparisons (exact *P* values are in the Source Data).

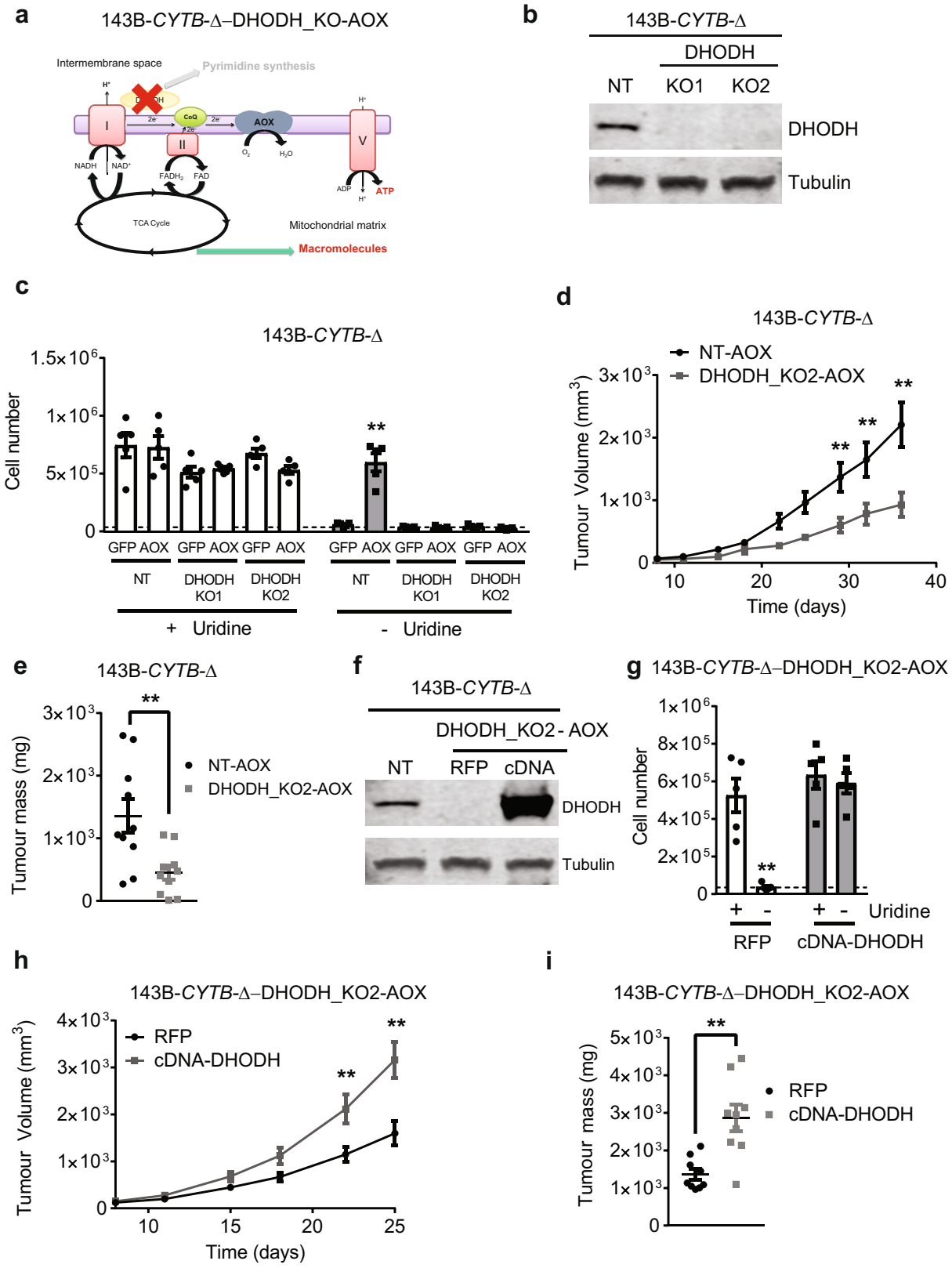

Extended Data Fig. 4 | See next page for caption.

Extended Data Fig. 4 | De novo pyrimidine synthesis is necessesary for tumour growth. a, Schematic representation of the ETC in 143B-*CYTB*-Δ–DHODH_KO-AOX cells. **b**, Western blot analysis of DHODH in 143B-*CYTB*-Δ non-targeting (NT) and 143B-*CYTB*-Δ-DHODH_KO cells. Tubulin was used as a loading control. Data are representative of two independent experiments. **c**, 143B-*CYTB*-Δ-NT or 143B-*CYTB*-Δ-DHODH-KOs expressing GFP or AOX were grown in the presence or absence of uridine and cell number was assessed after 72 h ($n = 5$ biologically independent experiments). **d**, **e**, Average tumour volume (**d**) and tumour mass (**e**) of xenografts from 143B-*CYTB*-Δ-NT-AOX and 143B-*CYTB*-Δ-DHODH_KO2-AOX cells ($n = 10$ mice per group from two independent cohorts). **f**, Western blot analysis of DHODH protein levels in 143B-*CYTB*-Δ-NT, 143B-*CYTB*-Δ-DHODH_KO2-AOX-RFP and 143B-*CYTB*-Δ-DHODH_KO2-AOX-cDNA DHODH cells. Data are representative of three independent experiments. **g**, 143B-*CYTB*-Δ-DHODH_KO2-AOX-RFP and 143B-*CYTB*-Δ-DHODH_KO2-AOX-cDNA DHODH cells were grown in the presence or absence of uridine and cell number was assessed after 72 h ($n = 5$ biologically independent experiments). **h**, **i**, Average tumour volume (**h**) and tumour mass (**i**) of xenografts from 143B-*CYTB*-Δ-DHODH_KO2-AOX-RFP and 143B-*CYTB*-Δ-DHODH_KO2-AOX-cDNA DHODH cells ($n = 9$ mice per group from two independent cohorts). Data are mean ± s.e.m. (**c**–**e**, **g**–**i**) $^{*}P < 0.05$, $^{**}P < 0.01$, two-tailed *t*-tests (**e**, **i**) or two-way ANOVA (**c**, **d**, **g**, **h**) with a Bonferroni test for multiple comparisons (exact *P* values are in the Source Data). For gel source data, see Supplementary Fig. 4.

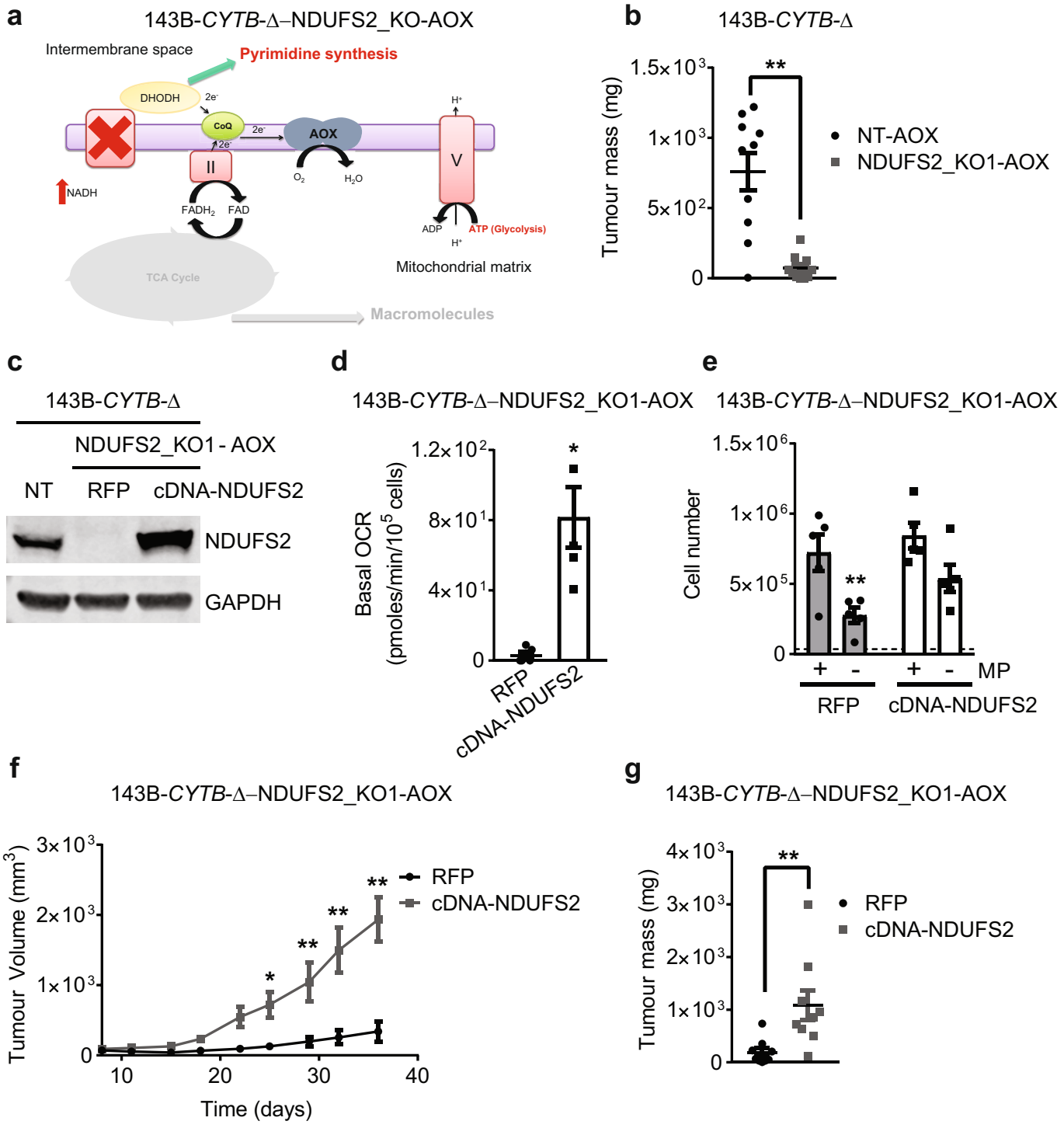

Extended Data Fig. 5 | Restoration of complex I by ectopic expression of *NDUFS2* cDNA rescues tumour growth. a, Schematic representation of the ETC in complex I-deficient 143B-*CYTB*-Δ-NDUFS2_KO-AOX cells. **b**, Tumour mass of xenografts from 143B-*CYTB*-Δ-NT-AOX and 143B-*CYTB*-Δ-NDUFS2_KO1-AOX cells ($n = 10$ mice per group from two independent cohorts). **c**, Western blot analysis of NDUFS2 protein levels in 143B-*CYTB*-Δ-NT cells, and in AOX-expressing 143B-*CYTB*-Δ-NDUFS2_KO1 clone transduced with either RFP or human *NDUFS2* cDNA. GAPDH was used as a loading control. Data representative of two independent experiments. **d**, Basal OCR of AOX expressing 143B-*CYTB*-Δ-NDUFS2_KO1 cells transduced with either RFP or human *NDUFS2* cDNA. **e**, 143B-*CYTB*-Δ-NDUFS2_KO1-AOX-RFP and 143B-*CYTB*-Δ-NDUFS2_KO1-AOX-cDNA NDUFS2 cells were grown in the presence or absence of methyl pyruvate and cell number was assessed after 72 h ($n = 5$ biologically independent experiments). **f**, **g**, Average tumour volume (**f**) and tumour mass (**g**) of xenografts from AOX-expressing 143B-*CYTB*-Δ-NDUFS2_KO1 cells transduced with either RFP or human *NDUFS2* cDNA ($n = 9$ mice per group from two independent cohorts). Data are mean ± s.e.m. (**b**, **d**–**g**). $^*P < 0.05$, $^{**}P < 0.01$, two-tailed *t*-tests (**b**, **d**, **g**) or two-way ANOVA (**e**, **f**) with a Bonferroni test for multiple comparisons (exact *P* values are in the Source Data). For gel source data, see Supplementary Fig. 2.

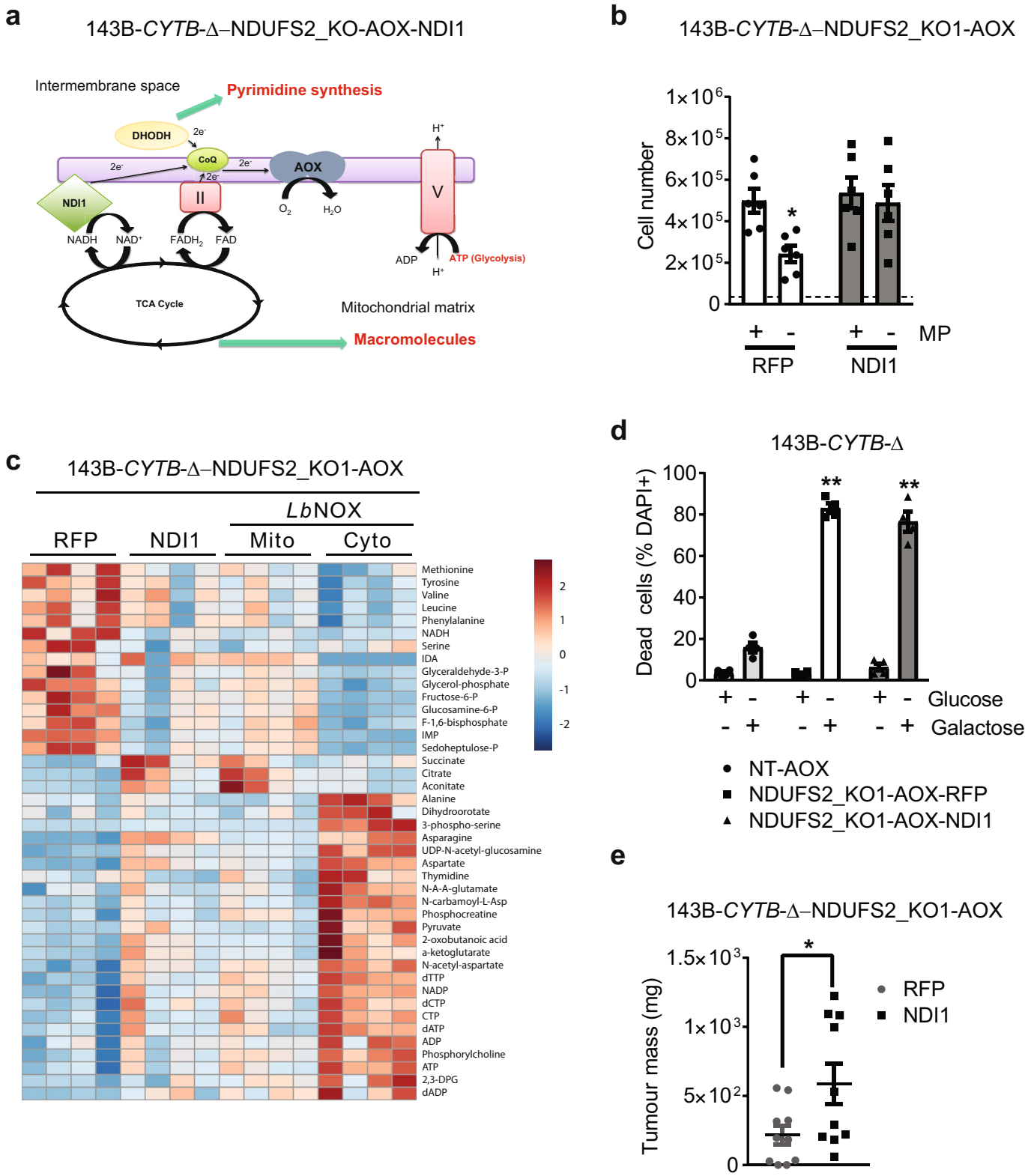

Extended Data Fig. 6 | See next page for caption.

Extended Data Fig. 6 | NDI1 expression in complex I-deficient cells rescues electron transfer but not ATP production. a, Schematic representation of the ETC in complex I deficient 143B-*CYTB*-Δ-NDUFS2_KO-AOX cells expressing NDI1. **b**, 143B-*CYTB*-Δ-NDUFS2_KO1-AOX-RFP and 143B-*CYTB*-Δ-NDUFS2_KO1-AOX-NDI1 cells were grown in the presence or absence of methyl pyruvate and cell number was assessed after 72 h ($n = 6$ biologically independent experiments). **c**, The heat map displays the relative abundance of significantly changed metabolites in 143B-*CYTB*-Δ–NDUFS2_KO1-AOX cells expressing RFP, NDI1 or *Lb*NOX in either mitochondria or cytosol ($n = 4$ biologically independent experiments). A red–blue colour scale depicts the abundance of the metabolites (red: high, blue: low). Metabolites levels were analysed with multiple one-way ANOVA using an FDR of 0.1 and Fisher's least significant difference test post hoc analyses $Q = 10\%$. Each row was analysed individually. (*$Q < 0.1$; exact Q values are in the Source Data.) **d**, 143B-*CYTB*-Δ-NT-AOX, 143B-*CYTB*-Δ-NDUFS2_KO1-AOX-RFP and 143B-*CYTB*-Δ-NDUFS2_KO1-AOX-NDI1 cells were grown in media containing 10 mM glucose or 10 mM galactose for 48 h and assessed for cell death ($n = 4$ biologically independent experiments). **e**, Tumour mass of xenografts from 143B-*CYTB*-Δ-NDUFS2_KO1 cells expressing AOX and either RFP or NDI1 ($n = 10$ mice per group from two independent cohorts). Data are mean ± s.e.m. (**b**, **d**, **e**). *$P < 0.05$, **$P < 0.01$, two-tailed t-tests (**e**) or two-way ANOVA (**b**, **d**) with a Bonferroni test for multiple comparisons (exact P values are in the Source Data).

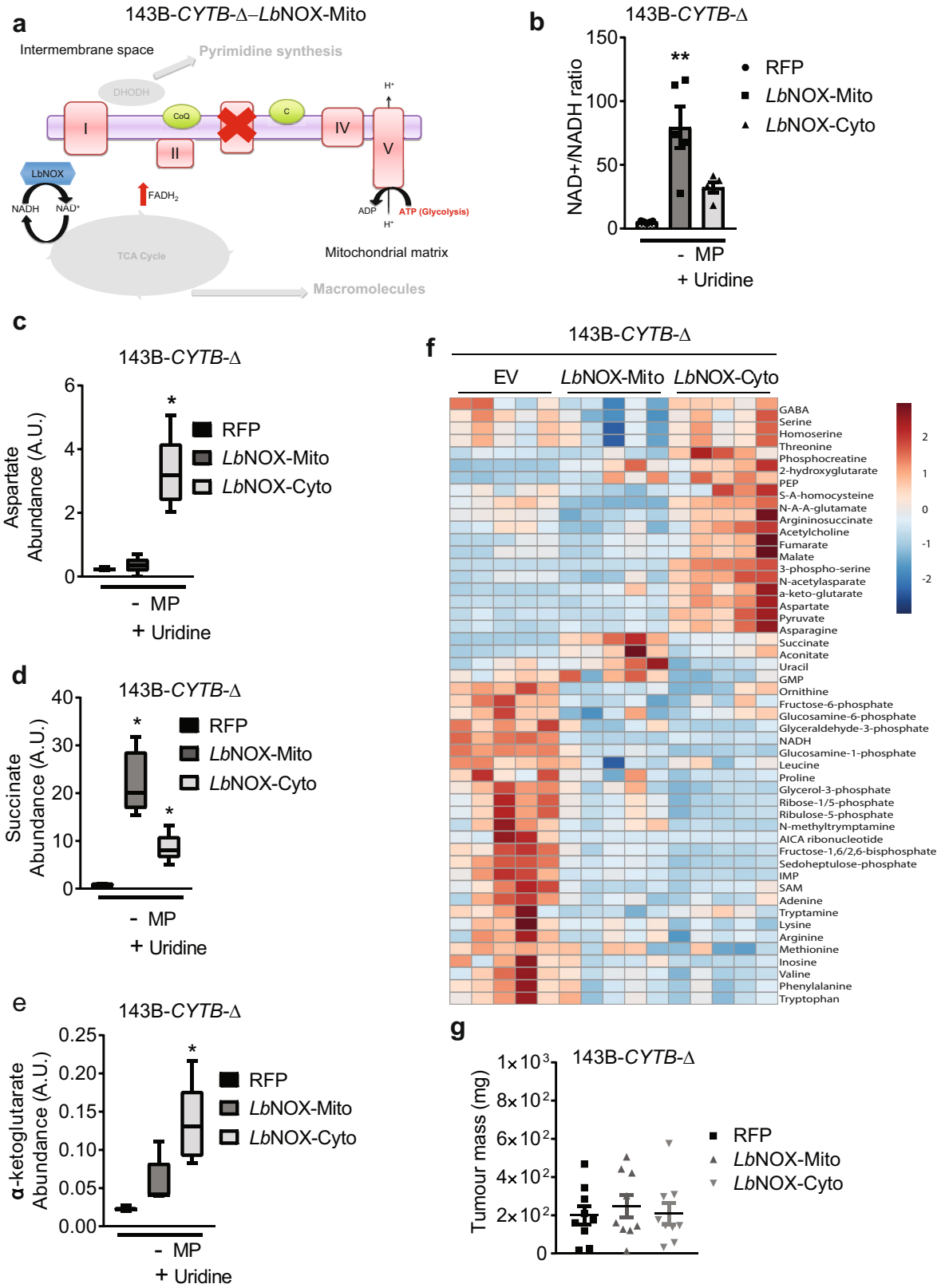

Extended Data Fig. 7 | See next page for caption.

Extended Data Fig. 7 | *Lb*NOX expression in mitochondria or cytosol promotes major changes in the metabolome of complex III-deficient cells. **a**, Schematic representation of the ETC in 143B-*CYTB*-Δ cells expressing *Lb*NOX in mitochondria. **b**, Intracellular NAD+/NADH ratio in 143B-*CYTB*-Δ-RFP, 143B-*CYTB*-Δ-*Lb*NOX-Mito and 143B-*CYTB*-Δ-*Lb*NOX-Cyto cells in the absence of methyl pyruvate ($n = 5$ biologically independent experiments). **c**–**e**, Intracellular aspartate (**c**), succinate (**d**) and α-ketoglutarate levels (**e**) in 143B-*CYTB*-Δ-RFP, 143B-*CYTB*-Δ-*Lb*NOX-Mito and 143B-*CYTB*-Δ-*Lb*NOX-Cyto cells in the absence of methyl pyruvate ($n = 5$ biologically independent experiments). **f**, The heat map displays the relative abundance of significantly changed metabolites in 143B-*CYTB*-Δ-RFP, 143B-*CYTB*-Δ-*Lb*NOX-Mito and 143B-*CYTB*-Δ-*Lb*NOX-Cyto cells in the absence of methyl pyruvate ($n = 5$ biologically independent experiments). A red–blue colour scale depicts the abundance of the metabolites (red: high, blue: low). **g**, Tumour mass of xenografts from 143B-*CYTB*-Δ-RFP, 143B-*CYTB*-Δ-*Lb*NOX-Mito and 143B-*CYTB*-Δ-*Lb*NOX-Cyto cells ($n = 9$ mice per group from two independent cohorts). Data are mean ± s.e.m. (**b**–**e**, **g**). $^{*}P < 0.05$, $^{**}P < 0.01$, one-way ANOVA (**b**, **g**) with a Bonferroni test for multiple comparisons (exact *P* values are in the Source Data). Metabolites levels (**c**–**f**) were analysed with multiple one-way ANOVA using an FDR of 0.1 and Fisher's least significant difference test post hoc analyses $Q = 10\%$. Each row was analysed individually ($^{*}Q < 0.1$; exact *Q* values in Source Data).

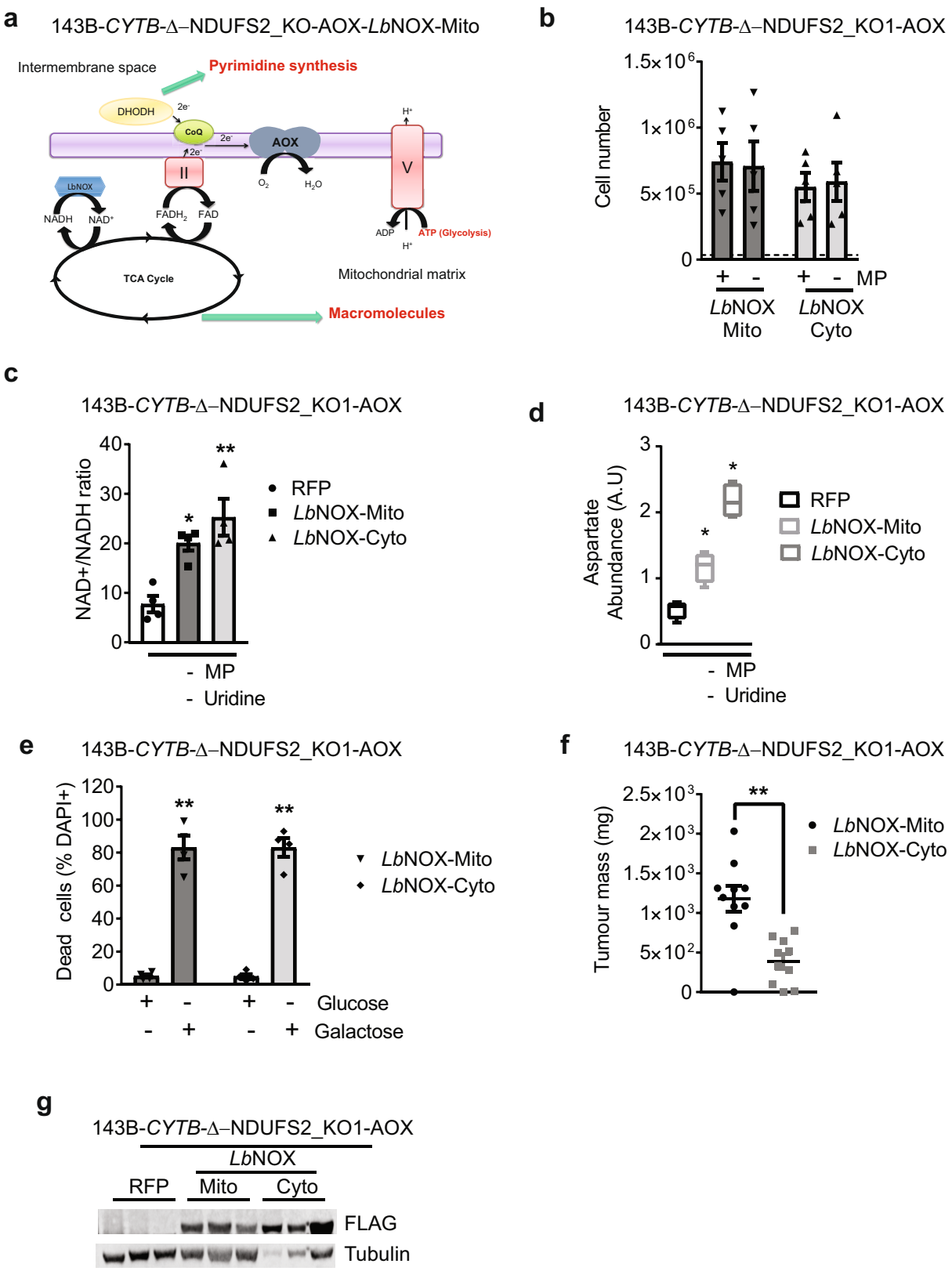

Extended Data Fig. 8 | See next page for caption.

Extended Data Fig. 8 | *Lb*NOX expression in mitochondria or cytosol promotes major changes in the metabolome of complex I deficient cells. **a**, Schematic representation of the ETC in 143B-*CYTB*-Δ-NDUFS2_KO-AOX cells expressing *Lb*NOX in mitochondria. **b**, 143B-*CYTB*-Δ-NDUFS2_KO1-AOX-*Lb*NOX-Mito and 143B-*CYTB*-Δ-NDUFS2_KO1-AOX-*Lb*NOX-Cyto were grown in the presence or absence of methyl pyruvate and cell number was assessed after 72 h ($n = 5$ biologically independent experiments). **c**, Intracellular NAD+/NADH ratio of 143B-*CYTB*-Δ-NDUFS2_KO1-AOX-RFP, 143B-*CYTB*-Δ-NDUFS2_KO1-AOX-*Lb*NOX-Mito and 143B-*CYTB*-Δ-NDUFS2_KO1-AOX-*Lb*NOX-Cyto cells in the absence of methyl pyruvate and uridine ($n = 4$ biologically independent experiments). **d**, Intracellular aspartate levels of 143B-*CYTB*-Δ-NDUFS2_KO1-AOX-RFP, 143B-*CYTB*-Δ-NDUFS2_KO1-AOX-*Lb*NOX-Mito and 143B-*CYTB*-Δ-NDUFS2_KO1-AOX-*Lb*NOX-Cyto cells in the absence of methyl pyruvate and uridine ($n = 4$ biologically independent experiments). **e**, 143B-*CYTB*-Δ-NDUFS2_KO1-AOX-*Lb*NOX-Mito and 143B-*CYTB*-Δ-NDUFS2_KO1-AOX-*Lb*NOX-Cyto cells were grown in medium containing 10 mM glucose or 10 mM galactose for 48 h and assessed for cell death ($n = 4$ biologically independent experiments). **f**, Tumour mass of xenografts from 143B-*CYTB*-Δ-NDUFS2_KO1-AOX cells expressing *Lb*NOX in either mitochondria or cytosol ($n = 10$ mice per group from two independent cohorts). **g**, Western blot analysis (data representative of two independent experiments) of *Lb*NOX expression in xenograft tumours from 143B-*CYTB*-Δ-NDUFS2_KO1-AOX-RFP, 143B-*CYTB*-Δ-NDUFS2_KO1-AOX-*Lb*NOX-Mito and 143B-*CYTB*-Δ-NDUFS2_KO1-AOX-*Lb*NOX-Cyto cells. Tubulin was used as a loading control. Data are mean ± s.e.m. (**b**–**f**). $^{*}P < 0.05$, $^{**}P < 0.01$, two-tailed *t*-tests (**f**), one-way ANOVA (**c**) with a Bonferroni test for multiple comparisons or a two-way ANOVA (**b**, **e**) with a Bonferroni test for multiple comparisons (exact *P* values are in the Source Data). Metabolites levels (**d**) were analysed with multiple one-way ANOVA using an FDR of 0.1 and Fisher's least significant difference test post hoc analyses $Q = 10\%$. Each row was analysed individually. ($^{*}Q < 0.1$; exact *Q* values in Source Data.) For gel source data, see Supplementary Fig. 5.

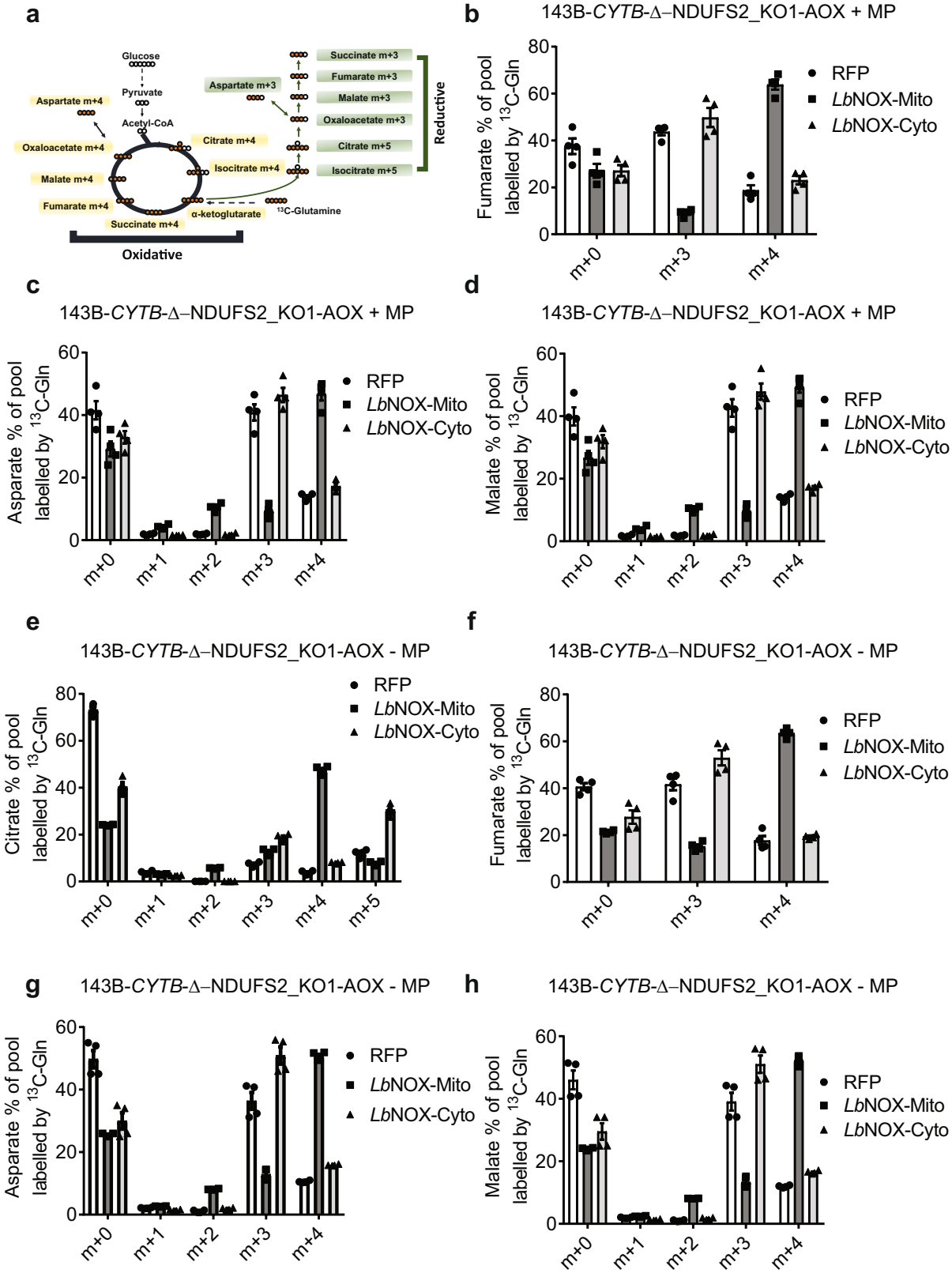

Extended Data Fig. 9 | Complex I-deficient cells expressing *Lb*NOX in the cytosol perform glutamine reductive carboxylation. a, Schematic representation for oxidative and reductive glutamine metabolism. Metabolism of [U-^{13}C]glutamine generates fully labelled α-ketoglutarate. Oxidation of α-ketoglutarate in the TCA cycle produces metabolites with four ^{13}C-carbons ($m+4$), while reduction of α-ketoglutarate through the reductive carboxylation pathway produces citrate with five ^{13}C-carbons ($m+5$). Further reductive metabolism of the $m+5$ citrate yields metabolites with three ^{13}C-carbons ($m+3$). **b**–**h**, 143B-*CYTB*-Δ-NDUFS2_KO1-AOX-RFP, 143B-*CYTB*-Δ-NDUFS2_KO1-AOX-*Lb*NOX-Mito and 143B-*CYTB*-Δ-NDUFS2_KO1-AOX-*Lb*NOX-Cyto cells were labelled for 6 h with [U-^{13}C]glutamine in the presence (**b**–**d**) or absence (**e**–**h**) of methyl pyruvate, and the percentage of labelled metabolite pools was examined. $m+5$ and $m+3$ pools result from glutamine flow through reductive metabolism. $m+4$ pools result from glutamine flow through oxidative metabolism. Data are mean ± s.e.m. of four biologically independent experiments.

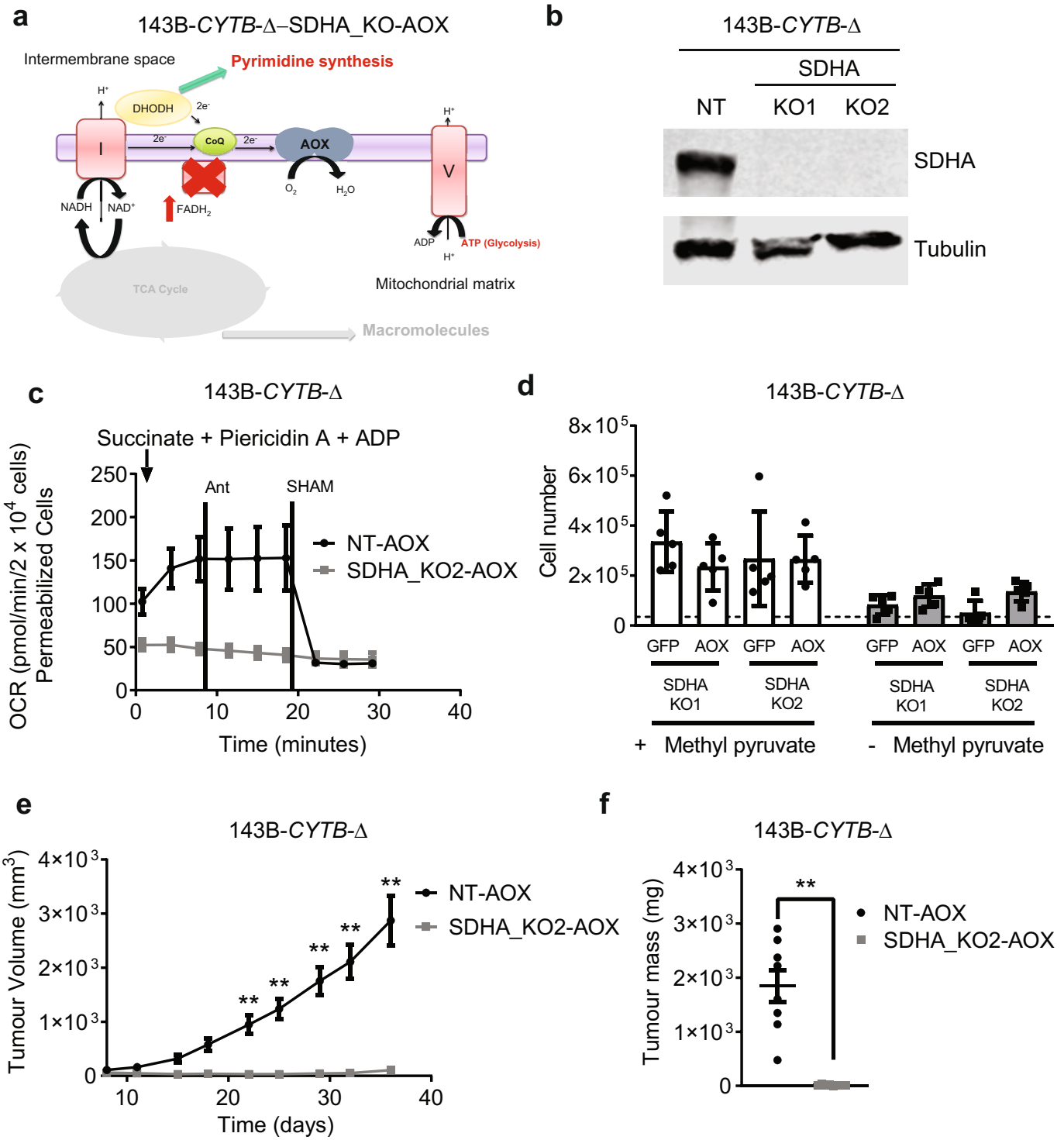

Extended Data Fig. 10 | Complex II is necessary for tumour growth. **a**, Schematic representation of the ETC in complex II deficient 143B-*CYTB*-Δ cells expressing AOX. **b**, Western blot analysis of SDHA in 143B-*CYTB*-Δ non-targeting and 143B-*CYTB*-Δ-SDHA_KO cells. Tubulin was used as a loading control. Data representative of two independent experiments. **c**, Complex II-driven OCR of permeabilized 143B-*CYTB*-Δ-NT-AOX and 143B-*CYTB*-Δ-SDHA_KO2-AOX cells. Piericidin A (1 µM) and antimycin A (1 µM) were used to inhibit complex I and III, respectively. SHAM (2 mM) was used to inhibit AOX activity ($n = 4$ biologically independent experiments). **d**, 143B-*CYTB*-Δ-SDHA-KOs expressing GFP or AOX were grown in the presence or absence of methyl pyruvate and cell number was assessed after 72 h ($n = 5$ biologically independent experiments). **e**, **f**, Average tumour volume (**e**) and tumour mass (**f**) of xenografts from 143B-*CYTB*-Δ-NT-AOX and 143B-*CYTB*-Δ-SDHA_KO2-AOX cells ($n = 8$ mice per group from two independent cohorts). Data are mean ± s.e.m. (**c**–**f**). $^*P < 0.05$; $^{**}P < 0.01$, two-tailed *t*-tests (**f**) or two-way ANOVA (**d**, **e**) with a Bonferroni test for multiple comparisons (exact *P* value are in the Source Data). For gel source data, see Supplementary Fig. 6.

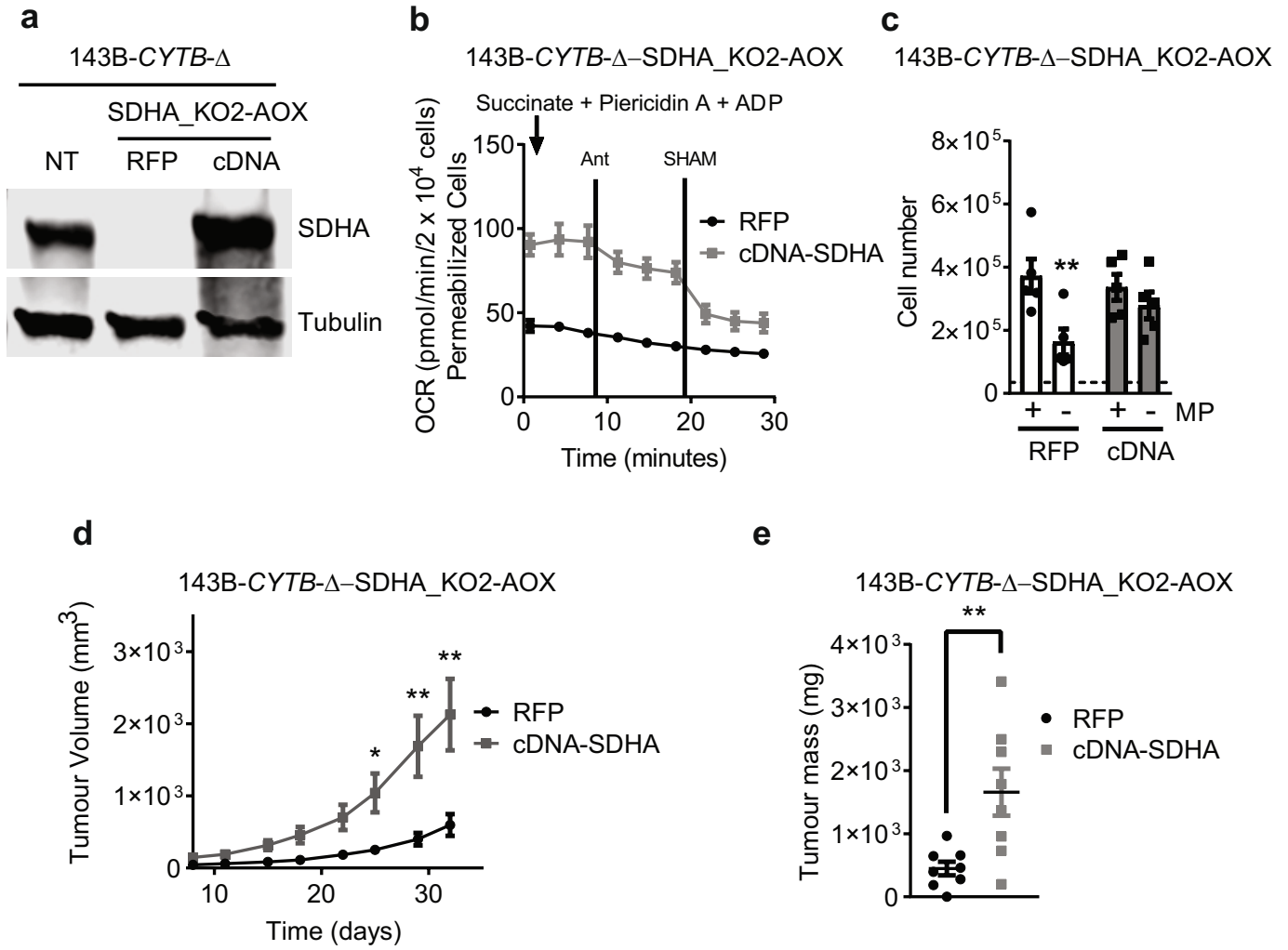

Extended Data Fig. 11 | Restoration of complex II by ectopic expression of *SDHA* cDNA rescues tumour growth. a, Western blot analysis of SDHA protein levels in 143B-*CYTB*-Δ-NT, 143B-*CYTB*-Δ-SDHA_KO2-AOX-RFP and 143B-*CYTB*-Δ-SDHA_KO2-AOX-cDNA SDHA cells. Data representative of three independent experiments. **b**, Complex II-driven OCR of permeabilized 143B-*CYTB*-Δ-SDHA_KO2-AOX-RFP and 143B-*CYTB*-Δ-SDHA_KO2-AOX-cDNA SDHA cells. Succinate and ADP were provided as substrates. Piericidin A (1 µM) and antimycin A (1 µM) were used to inhibit complex I and III respectively. SHAM (2 mM) was used to inhibit AOX activity ($n = 4$ biologically independent experiments). **c**, 143B-*CYTB*-Δ-SDHA_KO2-AOX-RFP and 143B-*CYTB*-Δ-SDHA_KO2-AOX-cDNA SDHA cells were grown in the presence or absence of methyl pyruvate and cell number was assessed after 72 h ($n = 5$ biologically independent experiments). **d**, **e**, Average tumour volume (**d**) and tumour mass (**e**) of xenografts from 143B-*CYTB*-Δ-SDHA_KO2-AOX-RFP and 143B-*CYTB*-Δ-SDHA_KO2-AOX-cDNA SDHA cells ($n = 8$ mice per group from two independent cohorts). Data are mean ± s.e.m. (**b**–**e**). $^*P < 0.05$, $^{**}P < 0.01$, two-tailed *t*-tests (**e**) or two-way ANOVA (**c**, **d**) with a Bonferroni test for multiple comparisons (exact *P* values are in the Source Data). For gel source data, see Supplementary Fig. 6.

nature research

Corresponding author(s): Navdeep S Chandel

Last updated by author(s): Mar 2, 2020

Reporting Summary

Nature Research wishes to improve the reproducibility of the work that we publish. This form provides structure for consistency and transparency in reporting. For further information on Nature Research policies, see Authors & Referees and the Editorial Policy Checklist.

Statistics

For all statistical analyses, confirm that the following items are present in the figure legend, table legend, main text, or Methods section.

n/a	Confirmed	
☐	☒	The exact sample size (*n*) for each experimental group/condition, given as a discrete number and unit of measurement
☐	☒	A statement on whether measurements were taken from distinct samples or whether the same sample was measured repeatedly
☐	☒	The statistical test(s) used AND whether they are one- or two-sided *Only common tests should be described solely by name; describe more complex techniques in the Methods section.*
☐	☒	A description of all covariates tested
☐	☒	A description of any assumptions or corrections, such as tests of normality and adjustment for multiple comparisons
☐	☒	A full description of the statistical parameters including central tendency (e.g. means) or other basic estimates (e.g. regression coefficient) AND variation (e.g. standard deviation) or associated estimates of uncertainty (e.g. confidence intervals)
☐	☒	For null hypothesis testing, the test statistic (e.g. *F*, *t*, *r*) with confidence intervals, effect sizes, degrees of freedom and *P* value noted *Give P values as exact values whenever suitable.*
☒	☐	For Bayesian analysis, information on the choice of priors and Markov chain Monte Carlo settings
☒	☐	For hierarchical and complex designs, identification of the appropriate level for tests and full reporting of outcomes
☒	☐	Estimates of effect sizes (e.g. Cohen's *d*, Pearson's *r*), indicating how they were calculated

Our web collection on statistics for biologists contains articles on many of the points above.

Software and code

Policy information about availability of computer code

Data collection	Oxygen consumption data was collected using Wave 2.4 software. Flow cytometry data was collected using FACS DIVA 8.0.3 software. Metabolite data was collected using Xcalibur 4.1 software. Luminescence values from the tumors were collected using the IVIS 4.5 or the LAGO 2.3.1 imaging systems. Western blot images were collected using Odyssey Fc Imaging System 5.2 From LI-COR.
Data analysis	GraphPad Prism 7.0 and MetaboAnalyst 4.0 were used for statistical tests. Flow cytometry data was analyzed using Flowjo 10.4.2. Metabolite data was analyzed using Tracefinder 4.1 software. Images from tumors were processed using the Living Image 4.5 or the Aura 2.3.1 softwares. Image Studio Lite version 5.0 (LI-COR) was used for the analysis of protein levels.

For manuscripts utilizing custom algorithms or software that are central to the research but not yet described in published literature, software must be made available to editors/reviewers. We strongly encourage code deposition in a community repository (e.g. GitHub). See the Nature Research guidelines for submitting code & software for further information.

Data

Policy information about availability of data

All manuscripts must include a data availability statement. This statement should provide the following information, where applicable:

- Accession codes, unique identifiers, or web links for publicly available datasets
- A list of figures that have associated raw data
- A description of any restrictions on data availability

Data from the manuscript are available from the corresponding author on request.

Field-specific reporting

Please select the one below that is the best fit for your research. If you are not sure, read the appropriate sections before making your selection.

☒ Life sciences ☐ Behavioural & social sciences ☐ Ecological, evolutionary & environmental sciences

For a reference copy of the document with all sections, see nature.com/documents/nr-reporting-summary-flat.pdf

Life sciences study design

All studies must disclose on these points even when the disclosure is negative.

Sample size	All the experiments were performed using sample sizes based on standard protocols in the field. We made an effort to avoid needless use of animals. No statistical test was performed to predetermine sample size. We used statistical analysis consistent with the sample size for each experiment and found sufficient statistical power with the sample sizes utilized in our study.
Data exclusions	For xenograft in vivo experiments, mice were excluded from the analysis if euthanasia had to be applied due to ulcerations or excessive tumor growth prior to the end point of the experiment. This exclusion criteria was pre-established.
Replication	All experimental data was reliably reproduced in multiple independent experiments as indicated in the figure legends. In vivo tumor experiments are from at least two independent cohorts to ensure reproducibility.
Randomization	Experimental animals were not randomized to experimental groups, but were age-matched, sex-matched, and littermates when possible.
Blinding	Investigators were not blinded. In case of leukemia studies blinding was not relevant, as groups consisted of previously genotyped mice in order to have correct experimental and control groups.

Reporting for specific materials, systems and methods

We require information from authors about some types of materials, experimental systems and methods used in many studies. Here, indicate whether each material, system or method listed is relevant to your study. If you are not sure if a list item applies to your research, read the appropriate section before selecting a response.

Materials & experimental systems

n/a	Involved in the study
☐	☒ Antibodies
☐	☒ Eukaryotic cell lines
☒	☐ Palaeontology
☐	☒ Animals and other organisms
☒	☐ Human research participants
☒	☐ Clinical data

Methods

n/a	Involved in the study
☒	☐ ChIP-seq
☐	☒ Flow cytometry
☒	☐ MRI-based neuroimaging

Antibodies

Antibodies used	Antibodies used for flow cytometry were: anti-Mouse Ter-119 (eBioscience; #48-5921-80; clone TER-119), anti-Mouse NK1.1 (eBioscience; #48-5941-80; clone PK136,), anti-Human/Mouse CD45R (B220) (eBioscience; #48-0452-80; clone RA3-6B2), anti-Mouse CD8a (eBioscience; #48-0081-82; clone 53-6.7), anti-Mouse CD11b (eBioscience; #48-0112-80; clone M1/70,), anti-Mouse Ly-6G (Gr-1) (eBioscience; #48-5931-80; clone RB6-8C5,), anti-Mouse CD4 (Tonbo Biosciences; #75-0041-U100; clone GK1.5). Antibodies used for western blots were: anti-NDUFS2 (Abcam; #ab103024; 1:500 dilution), anti-QPC (Abcam; #ab136679; 1:500 dilution), anti-SDHA (MitoScience; #MS204; clone 2E3GC12FB2AE2; 1:500 dilution), anti-DHODH (Santa Cruz; #sc-166348; clone E-8; 1:500 dilution), anti-FLAG (Sigma; #F1804; clone M2; 1:1000 dilution), anti-GAPDH (Santa Cruz; #sc-32233; clone 6C5, and Sigma; #G9545; 1:2000 dilution), anti-ATP5A (Mitosciences; #MS507; clone 15H4C4; 1:1000 dilution), anti-Tubulin (Cell Signaling; #2144; 1:1000 dilution) and anti-β-Actin (Sigma; # A2228-100UL; clone AC-74,).
Validation	The antibodies used in this study were tested by the manufacturer. Antibodies used for flow citometry: - anti-Mouse Ter-119 (clone number: TER-119 eBioscience; catalogue number: 48-5921-80). This antibody has been used in 25 published figures and can be found in 42 references. The manufacturer also provides antibody testing data. https://www.thermofisher.com/antibody/product/TER-119-Antibody-clone-TER-119-Monoclonal/48-5921-80 - anti-Mouse NK1.1 (clone number: PK136, eBioscience; catalogue number: 48-5941-80). This antibody has been used in 27

published figures and can be found in 28 references. The manufacturer also provides antibody testing data. https://www.thermofisher.com/antibody/product/NK1-1-Antibody-clone-PK136-Monoclonal/48-5941-80

- anti-Human/Mouse CD45R (B220) (clone number: RA3-6B2, eBioscience; catalogue number: 48-0452-80). This antibody has been used in 40 published figures and can be found in 95 references. The manufacturer also provides antibody testing data and advanced verification by relative expression to ensure that the antibody binds to the antigen stated. https://www.thermofisher.com/antibody/product/CD45R-B220-Antibody-clone-RA3-6B2-Monoclonal/48-0452-80

- anti-Mouse CD8a (clone number: 53-6.7, eBioscience, catalogue number: 48-0081-82). This antibody has been used in 40 published figures and can be found in 138 references. The manufacturer also provides antibody testing data. https://www.thermofisher.com/antibody/product/CD8a-Antibody-clone-53-6-7-Monoclonal/48-0081-82

- anti-Mouse CD11b (clone number: M1/70, eBioscience; catalogue number: 48-0112-80). This antibody has been used in 40 published figures and can be found in 230 references. The manufacturer also provides antibody testing data. https://www.thermofisher.com/antibody/product/CD11b-Antibody-clone-M1-70-Monoclonal/48-0112-80

- anti-Mouse Ly-6G (Gr-1) (clone number: RB6-8C5, eBioscience; catalogue number: 48-5931-80). This antibody has been used in 40 published figures and can be found in 102 references. The manufacturer also provides antibody testing data and advanced verification by relative expression to ensure that the antibody binds to the antigen stated. https://www.thermofisher.com/antibody/product/Ly-6G-Ly-6C-Antibody-clone-RB6-8C5-Monoclonal/48-5931-80

- anti-Mouse CD4 (clone number: GK1.5, Tonbo Biosciences; catalogue number: 75-0041-U100). Tonbo Biosciences tests all antibodies by flow cytometry. https://tonbobio.com/products/violetfluor-450-anti-mouse-cd4-gk1-5

Antibodies used for western blots:

- anti-NDUFS2 (Abcam; catalogue number: ab103024; used at a 1:500 dilution). The Abpromise guarantee covers the used of the antibody for WB application. However, the antibody is not available anymore. https://www.abcam.com/ndufs2-antibody-ab103024.html

- anti-QPC (Abcam; catalogue number: ab136679; used at 1:500 dilution). The Abpromise guarantee covers the used of the antibody for WB application. https://www.abcam.com/uqcrq-antibody-ab136679.html#top-294

- anti-SDHA (clone number: 2E3GC12FB2AE2, MitoScience; catalog number: MS204; used at a 1:500 dilution). The Abpromise guarantee covers the used of the antibody for WB application. This antibody has been referenced in 235 publications. https://www.abcam.com/sdha-antibody-2e3gc12fb2ae2-ab14715.html#top-701

- anti-DHODH (clone number: E-8, Santa Cruz; catalog number: sc-166348; used at a 1:500 dilution). This antibody has been referenced in 5 publications. The manufacturer also provides antibody testing data. https://datasheets.scbt.com/sc-166348.pdf

- anti-FLAG (clone number: M2, Sigma; catalog number: F1804; used at a 1:1000 dilution). This antibody has been referenced in 4024 publications. The manufacturer also provides antibody testing data. https://www.sigmaaldrich.com/catalog/product/sigma/f1804?lang=en&region=US

- anti-GAPDH (clone number: 6C5, Santa Cruz; catalog number: sc-32233 and Sigma; catalog number: G9545; used at a 1:2000 dilution). For sc-32233 antibody from Santa Cruz, the antibody has been referenced in 2479 publications. The manufacturer also provides antibody testing data. https://datasheets.scbt.com/sc-32233.pdf. For G9545 from Sigma, the antibody has been referenced in 792 publications. The manufacturer also provides antibody testing data. https://www.sigmaaldrich.com/catalog/product/sigma/g9545?lang=en&region=US

- anti-ATP5A (clone number: 15H4C4, Mitosciences; catalog number: MS507; used at a 1:1000 dilution). The Abpromise guarantee covers the used of the antibody for WB application. The antibody has been referenced in 243 publications. The manufacturer also provides antibody testing data. https://www.abcam.com/atp5a-antibody-15h4c4-mitochondrial-marker-ab14748.html

- anti-Tubulin (Cell Signaling; catalog number: 2144, used at a 1:1000 dilution). This antibody has been referenced in 341 publications. The company tested that The α-Tubulin Antibody detects endogenous levels of total α-tubulin protein, and does not cross-react with recombinant β-tubulin. https://www.cellsignal.com/products/primary-antibodies/a-tubulin-antibody/2144

- anti-β-Actin (clone number: AC-74, Sigma; catalog number: A2228-100UL). This antibody has been referenced in 1412 publications. The manufacturer also provides antibody testing data. https://www.sigmaaldrich.com/catalog/product/sigma/a2228?lang=en&region=US

Eukaryotic cell lines

Policy information about cell lines

Cell line source(s)	143B-Cytb-WT and 143B-Cytb-Δ cells were previously described (Weinberg et al. PNAS. 2010). Mouse KrasG12D p53-/- (KP) lung tumor cells expressing luciferase were generously provided by Dr. T. Papagiannakopoulos. 293T were from ATCC. Platinum E-retroviral packaging cells were a kind gift from Dr. P. Ntziachristos.
Authentication	Neither of the cell lines used were authenticated.

Mycoplasma contamination	Cell lines tested negative for mycoplasma contamination. Cells were checked periodically.
Commonly misidentified lines (See ICLAC register)	These cell lines are not listed in the database of commonly misidentified cell lines maintained by ICLAC.

Animals and other organisms

Policy information about studies involving animals; ARRIVE guidelines recommended for reporting animal research

Laboratory animals	For leukemia experiments we used C57BL/6 Uqcrq (QPC null/wt or QPC null/fx) that have been recently described (Weinberg et al. Nature 2019). Uqcrq (QPC) floxed (Fx), wildtype (WT) and null (-) alleles were genotyped using the following primers: QPC-F: CTTCCGCTCCTCCCGGAAGT, QPC-R: TTCCCAAACTCGCGGCCCATG and QPC-null: CAATTCCAGCCAACAGTCCC. Ubc-CreERT2 mice were obtained from the Jackson Laboratory. Wild-type C57Bl/6 were used as recipients for T-ALL experiments. 8 to 12 weeks old mice of both sexes were used for experiments. For xenograft tumor studies, we used male J:Nu mice (8 to 12 weeks) obtained from Jackson Laboratory. For the orthotopic lung tumor model, we used male C57BL/6 mice (8 to 12 weeks).
Wild animals	This study did not involve wild animals.
Field-collected samples	This study did not involve samples collected from the field.
Ethics oversight	All mouse work was done in accordance with Northwestern University Institutional Animal Care and Use Committee (IACUC).

Note that full information on the approval of the study protocol must also be provided in the manuscript.

Flow Cytometry

Plots

Confirm that:

☐ The axis labels state the marker and fluorochrome used (e.g. CD4-FITC).

☐ The axis scales are clearly visible. Include numbers along axes only for bottom left plot of group (a 'group' is an analysis of identical markers).

☐ All plots are contour plots with outliers or pseudocolor plots.

☒ A numerical value for number of cells or percentage (with statistics) is provided.

Methodology

Sample preparation	Sample preparation is described in detail in the methods section of the manuscript. Briefly, for T-ALL experiments, lineage (CD4, CD8a, B220, CD11b, Gr-1, NK1.1, Ter-119)-negative, and GFP+ bone marrow cells transduced with the Notch1ΔE-GFP retrovirus were sorted on BD FACS Aria systems. To asses tumor burden, spleen, and one set of pelvis, femur, and tibia were harvested from each recipient, and analyzed for the number and % of GFP+ T-ALL cells, using PKH reference microbeads (Sigma). Samples were harvested from adult mice. To obtain a single-cell suspension, tissues were disrupted using scored 60mm petri dishes in PBS containing 2% FBS and filtered through a 70µM nylon mesh filter. Expression of GFP was analyzed using BD FACSymphony. For in vitro proliferation experiments, supernatant containing dead cells and cells attached to the wells were collected and centrifuged at 300 × g for 5 min. AccuCount Fluorescent Particles from Spherotech were added to count the cells. Cell viability was assessed by DAPI staining. Numerical values for number of cells or percentage with statistics for each graph is provided in Source Data files.
Instrument	BD LSR Fortessa, BD FACSymphony or BD FACSAria cell sorter.
Software	BD FASC Diva was used for collection of the data. All data was analyzed using FlowJo software.
Cell population abundance	The cells were periodically sorted to maintain high protein expressions. An aliquot of the sorted cells were always collected and run on a cytometer to verify purity of the samples collected. In addition, cell counts were performed on samples post sort to verify correct cell numbers.
Gating strategy	A supplemental figure is provided to show the gating strategy for T-ALL burden analysis. 2 different analysis were done: # of GFP+ Cells: Used the following flow plots to obtain: SSC-A vs. FSC-A: count of Lymphocytes --> A FSC-H vs. PE-A: count of PKH beads --> B APC-Cy7-A vs. BB515-A (showing the Lymphocytes population): % of GFP+ and Live lymphocytes --> C Actual # of lymphocytes = (A / B) x PKH bead concentration (in beads/ml, counted using hemocytometer each time) x total volume of cell suspension (ml) # of GFP+ cells = Actual # of lymphocytes x C

% of GFP+ Cells:
SSC-A vs. FSC-A: Lymphocytes population
FSC-H vs. FSC-A (showing the Lymphocytes population): Singlet population
SSC-H vs. APC-Cy7-A (showing the Singlet population): Live population
SSC-H vs. BB515-A (showing the live population): % of GFP+ population --> D
% GFP+ Cells = D

For proliferation experiments, beads and cells were identified first by discrimination by size (FSC-A by SSC-A). Singlets were then distinguished using FSC-A by FSH-H. Beads and Live cells were further gated by the appropiate fluorochrome used.

☒ Tick this box to confirm that a figure exemplifying the gating strategy is provided in the Supplementary Information.